

Chapter 4

ACCRETION ONTO SUPERMASSIVE BLACK HOLES IN QUASARS: LEARNING FROM OPTICAL/UV OBSERVATIONS

Paola Marziani¹, Deborah Dultzin-Hacyan² and Jack W. Sulentic³

¹Istituto Nazionale di Astrofisica, Osservatorio Astronomico di Padova,
Vicolo dell'Osservatorio 5, I-35122 Padova, Italia

²Instituto de Astronomía, Universidad Nacional Autónoma de México,
Apartado postal 70-264, 4510 México, D.F., México,

³Department of Physics & Astronomy, University of Alabama,
Tuscaloosa, AL 35487, USA

Abstract

Accretion processes in quasars and active galactic nuclei are still poorly understood, especially as far as the connection between observed spectral properties and physical parameters is concerned. Quasars show an additional degree of complexity compared to stars that is related to anisotropic emission/obscuration influencing the observed properties in most spectral ranges. This complicating factor has hampered efforts to define the equivalent of an Hertzsprung-Russel diagram for quasars. Even if it has recently become possible to estimate black hole mass and Eddington ratio for sources using optical and UV broad emission lines, the results are still plagued by large uncertainties. Nevertheless, robust trends are emerging from multivariate analysis of large spectral datasets of quasars. A firm observational basis is being laid out by accurate measurements of broad emission line properties especially when the source rest-frame is known. We consider the most widely discussed correlations (i.e. the so-called “eigenvector 1 parameter space” and the “Baldwin effect”) and analyze how they can be explained in terms of accretion properties, broad line region structure, and source evolution. We critically review recent estimates of black hole mass, accretion rate, spin and possible orientation indicators, stressing that any improvement in these parameters will provide a much better understanding of the physics and dynamics of the region producing the optical and UV broad emission lines. More accurate measurements of Eddington ratio and black hole mass may have a significant impact on

our ideas about evolution of quasar properties with redshift and luminosity as well as on broader cosmological issues.

1 Introduction

Tremendous data gathering advancements make now possible to see a distant solution for most of the deepest conundrums concerning quasar research. There has been an exponential growth in the number of known quasars lasting since the 1970s. Presently, the 11th edition of the Véron-Cetty & Véron Catalogue of AGNs and quasars [253] lists ≈ 50000 quasars. The *Sloan Digital Sky Survey* (SDSS) plans to compile a sample of ~ 100000 quasars. The SDSS Third Data Release provides *Charge Coupled Device* (CCD) spectra for 51000 quasars found over 4200 deg^2 [210]. The improvement in observational capabilities has been possible by the introduction and spread of CCDs and other linear, high detective quantum efficiency devices as detectors for astronomical observations since the late 1980s. At a second stance comes the increase in access to large light-gathering power telescopes of aperture $\gtrsim 4\text{m}$, crucial for spectroscopic observations. The ability to carry out multi-frequency observations with increasing spectral resolution and sensitivity (most notably provided by *Hubble Space Telescope* (HST) and by the *Far Ultraviolet Spectroscopic Explorer* (FUSE) for the optical/UV) through the 1990s and early 2000s has been a third factor of relevance. The data gathering improvements – which are the foundation of every astronomical advancement – have led to the discovery of systematic trends in quasar properties. These suggest that quasars are *not* well described by an average spectrum. We can amplify this statement to say that the spectra of quasars seen at a fixed viewing angle are also not the same – the basic tenet of Unification Schemes [1]. Yet, data have not been fully digested in physical terms. Observational constraints have been only very recently organized in meaningful ways. We still lack the ability to derive important physical information from observational parameters on an object-by-object basis. The first aim of this paper is to set the point of our present knowledge on the diversity of quasar spectral properties, especially in the optical and UV spectral ranges (§ 2). We then discuss much needed improvement to ensure accurate measurements of the main physical parameters (§ 4) as well as structural constraints on the line emitting regions (§ 3) and the physical basis of quasar diversity (§ 5, § 7, § 8).

1.1 Basic Accretion Parameters

We regard quasars and active galactic nuclei as systems accreting matter onto a massive ($\gtrsim 10^5 M_\odot$) black hole (see §1.3 for possible caveats). The main parameters are, as for any accreting system, black hole mass (M_{BH} , §4), Eddington ratio (§7), and mass accretion rate \dot{M} in $M_\odot \text{ yr}^{-1}$. The Eddington ratio $L_{\text{bol}}/L_{\text{Edd}}$ is defined as the ratio between the AGN bolometric luminosity L_{bol} and the Eddington luminosity L_{Edd} , i.e., the limiting luminosity beyond which radiation pressure overcomes gravitational attraction if accretion is spherical [177]. The Eddington luminosity is directly proportional to M_{BH} , and can be

written as

$$L_{\text{Edd}} \approx 1.3 \times 10^{38} (M_{\text{BH}}/M_{\odot}) \text{ ergs s}^{-1}.$$

Since the power emitted by an active nucleus through conversion of mass into energy can be expressed as $L_{\text{bol}} = \eta \dot{M} c^2$, it is possible to define an Eddington accretion rate $\dot{M}_{\text{Edd}} = L_{\text{Edd}}/(\eta c^2)$, and hence a dimensionless accretion rate $\dot{m} = \dot{M}/\dot{M}_{\text{Edd}}$. We stress that $L_{\text{bol}}/L_{\text{Edd}} \propto L_{\text{bol}}/M_{\text{BH}}$, and that $L_{\text{bol}}/M_{\text{BH}}$ is a quantity that can be derived from observations. On the other hand, the value of the efficiency η (~ 0.1) depends on the accretion mode which may not be the same for all sources: if matter is confined in an accretion disk as it is customarily assumed [211], η depends on the geometry and radiative properties of the disk, which in turn may depend on \dot{M} . Therefore we will not always confuse the dimensionless accretion rate \dot{m} and the Eddington ratio as it is frequently done in literature: for a fixed efficiency, there could be well super-Eddington accretion even if the source is radiating at, or below, the Eddington limit [41]. Black hole spin (§5) and an orientation angle (defined as the angle between the line of sight and the axis of the accretion disk around the black hole θ , §5.2) probably matter in the context of UV/optical properties although they have turned out to be very elusive to measure.

1.2 Nomenclature and Samples

We use the word quasar here in a generic fashion which means all classes of extragalactic objects that show *broad* (full width at half maximum, $\text{FWHM} \gtrsim 1000 \text{ km s}^{-1}$) optical and UV emission lines. This includes the nuclei of Seyfert and broad-line radio galaxies (BLRG) as well as radio-quiet (RQ) and radio-loud (RL) optically unresolved sources. They are often referred to under the umbrella of *Active Galactic Nuclei* (AGNs) which reinforces the paradigm that they are driven by the same physics differing only in their redshift-implied distances and, hence, luminosity. At the same time, there is no divide in AGN occurrence at the canonical boundary (absolute B magnitude $M_{\text{B}} \approx 22.5$ for $H_0 \approx 65 \text{ km s}^{-1} \text{ Mpc}^{-1}$) that separates Seyfert nuclei from quasars [253], so that nomenclature may be kept luminosity-independent. For instance, we keep using the word Narrow Line Seyfert 1 (§2.7) for sources that are actually luminous quasars.

Most sources considered in this review were “classically” selected through color criteria. Major color-based surveys include the *Palomar-Green* (PG), the *Large Bright Quasar Survey* (LBQS), the *ESO-Hamburg* (HE) quasar survey and the SDSS. The SDSS photometric system was designed to allow quasars at $0 \lesssim z \lesssim 6$ to be identified with multicolor selection techniques [208]. Other high-quality data-sets, even if more heterogeneous and less complete, are also considered [22, 50, 89, 140, 212, 277], especially if spectral resolution $\lambda/\Delta\lambda \sim 1000$ and continuum $S/N \gtrsim 20$. These samples often include ~ 100 objects of “good” spectra; studies on the LBQS involve $\sim 10^3$ sources, while the SDSS accounts for another order of magnitude leap in sample size, with $\sim 10^4$ sources.

No consideration to obscured AGNs will be given since the very possibility of accretion parameter estimation from the observed optical/UV quasar spectra turns out to be related

to the measurement of quasar broad emission line shifts, profile widths, and equivalent widths. Quasars showing broad lines are often referred to as “type-1” AGNs to distinguish them from Seyfert 2 nuclei and type 2 quasars (see e.g., Refs. [1, 173]) which will not be considered here.

There are more cumbersome, borderline AGNs which could be grouped into three classes:

1. sources that show very large broad Balmer intensity decrement $H\alpha/H\beta \gtrsim 7$ [61]. Objects of this kind often show dramatic differences between the broad component of $H\alpha$ and $H\beta$, and are not always found in color-based surveys. RL AGNs hosted in early-type galaxies like Pictor A are among them [228].
2. An analysis of spectra of quasars in the *Half-Jansky Parkes Survey* [76] suggests that the wide majority ($\approx 80\%$) are sources whose continuum is dominated by a pure power-law spectrum ($f_\nu \propto \nu^{0.5-2}$) ascribed to synchrotron radiation. These sources show broad lines and are bona-fide type-1 sources although their equivalent width is somewhat lower than that expected for color-selected quasars (see also §7). Sources with rather low $W(H\beta_{BC})$ and very broad $HeII\lambda 4686$ (most notably NGC 1275, indeed a core-dominated BRLG) may be seen as somewhat peculiar with respect to the other AGNs, especially if an important goal of the spectral analysis is M_{BH} measurements.
3. A third class of sources may show contamination in the nuclear spectrum of emission components associated to strong star formation. At the very least, the bolometric luminosity can be significantly affected as in the case of Mkn 231 [26, 53, 225]. Circumnuclear starbursts do occur in Seyfert 1 sources and quasars [93, 102, 57], and are usually *not* resolved. The emission line spectra of luminous Seyfert 1 nuclei may well be affected by the absorption/emission features observed in strong wind galaxies (e.g. NGC 4691; [81]). *Broad Absorption Lines* (BAL) observed in quasars could be associated to nova stars [219].

We mention these three AGN optical/UV spectral typologies since they may be extremes of AGNs accretion parameters, especially of L_{bol}/L_{Edd} (§4, §7): sources in the third class are likely to be “young” quasars radiating at high L_{bol}/L_{Edd} ; the first class may include “dying” quasars radiating at very low L_{bol}/L_{Edd} with little reservoir of matter (§8.3).

1.3 Rationale for a Black Hole in Active Galactic Nuclei

Do we have a definitive proof that the central massive object at the center of quasar is a black hole? From the definition of event horizon ($R_g = 2GM/c^2$ for a non-rotating black hole, where G is the gravitational constant), the mass of the black hole must satisfy the condition $M_{BH}/R_g \gtrsim 6.7 \cdot 10^{27} \text{ g cm}^{-1}$. Although this criterion has not been satisfied yet by observations of extragalactic sources, circumstantial evidence in favor of a black hole is

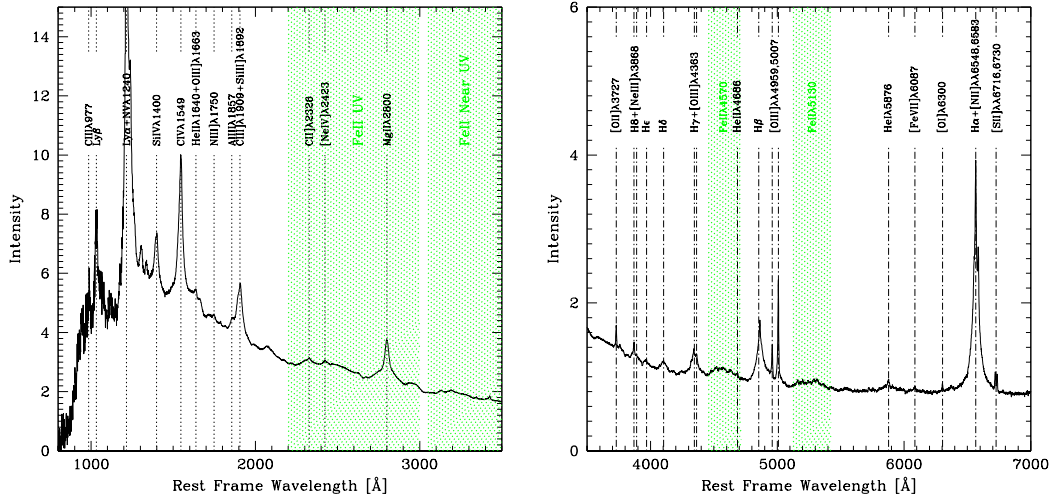


Figure 1: SDSS median composite spectrum, in the UV (left panel) and in the optical spectral range (right panel). Major features are identified; regions with strong emission blends of FeII are shaded. For a more exhaustive line list see Ref. [247].

now considered overwhelming [16]. From the time delay in the response of emission lines to continuum variations (“reverberation mapping”) it is possible to estimate the central mass assuming that the line broadening is due to Doppler effect, and to test whether the emitting gas motion is virial. In luminous Seyfert 1 galaxies, the central mass can be $\sim 10^8 M_{\odot}$ within the emitting region of the broad lines (the “Broad Line Region”, BLR) size, of the order of 1 light month. The resulting $M_{\text{BH}}/r_{\text{BLR}} \sim 10^{24} \text{ g cm}^{-1}$ is far less than the M_{BH}/r requirement for a black hole. However, time responses for lines of different width are roughly consistent with a Keplerian trend i.e., with a “point-like” mass concentration with respect to the BLR size [123]. It is therefore legitimate to talk at the very least about “compact massive objects” at the center of AGNs. This would be a proper, observation-bounded definition. We will use the term black hole with the reassurance of a large body of circumstantial evidence as well as with the perspective of decisive tests. In addition, most of the reasoning presented in this paper is largely independent on the exact nature of the “compact massive object,” provided that it is really compact and massive.

2 Eigenvector 1

2.1 Quasar Surveys and Quasar Spectral Diversity

Fig. 1 shows a median composite quasar spectrum, between 800 Å and 7000 Å, with sources spanning a redshift range $0.044 < z < 4.789$. The spectrum was obtained using a homogeneous data set of over 2200 spectra from the SDSS, at a resolution $\lambda/\Delta\lambda \approx 1800$. It reaches

a peak signal-to-noise ratio (S/N) of over 300 per 1 Å resolution element in the rest frame. See Ref. [247] for a comprehensive line list of 80 emission features. Similar composite spectra have been recently constructed from HST *Faint Object Spectrograph* and FUSE observations [209, 290]. The main advantage of composite spectra is that S/N is so high that identification of many faint features that remain invisible in individual spectra becomes possible [77]. Most prominent features and overall continuum shape are easily appreciable; from Fig. 1 one can realize the extent of FeII emission (shaded areas), the prominence of hydrogen Balmer (especially broad H α , H β , H γ), of Lyman lines, and of the CIV λ 1549 line, which makes them, apart from their physical importance, the best studied optical/UV lines of AGNs. Beyond line identification and some basic information a composite spectrum can yield deceptive results. In principle it is legitimate to median together all spectra of a given survey if spectral properties scatter randomly with reasonable dispersion around the median. This is not the case for color selected samples of quasars. It is important to remark that attempts to model a composite spectrum like the ones from the SDSS and LBQS [77, 247] may be doomed to failure. Ionization conditions and gas kinematics are not the same for all type-1 AGNs [139]. The use of average line ratios from composite survey spectra has led to an impasse in the attempt at reproducing the observations through simple photoionization models (see e.g., Ref. [170], and references therein), an impasse that still hampers present-day efforts. Recent high quality data [212] with nearly simultaneous FUSE, HST and optical observations emphasize the quasar diversity in terms of emission line and continuum spectrophotometric properties. Optical data for ≈ 200 AGNs at $z \lesssim 0.8$ obtained with resolution $\lambda/\Delta\lambda \sim 1000$ show the impressive diversity in terms of emission line profiles [140].

2.2 Basis of Eigenvector Analysis

Eigenvector techniques are applied whenever many variables appear to be more or less loosely correlated without an intuitive indication of a dominant correlation or variable. A set of n objects may have m measured parameters like flux, FWHM, and equivalent widths of optical and UV emission lines, continuum shape, etc. We can think that each set of measurement is a vector in an m -dimensional space described by orthogonal vectors \vec{v} , and define a matrix M of n vectors with m measurements. The *Principal Component Analysis* (PCA) searches for the best-fitting set of orthogonal axes to replace the original m axes in the space of measured parameters. The new axis set is sought by maximizing the sum of the squared projections onto each axis i.e., $(M\vec{v})^T(M\vec{v})$, where M^T denotes the transposed matrix. If the set of measurements has been previously centered subtracting the variable average, then $M^T M$ can be thought as a variance/covariance matrix. In spectral PCA no measurements are performed: the whole spectrum of n objects is divided into m small wavelength bins, and each input variable is the flux in the wavelength bin [213, 285]. We seek the maximum of $\vec{v}^T M^T M \vec{v}$ imposing the condition that the norm of \vec{v} is unity through a Lagrange multiplier λ , and setting the first derivative to 0 [156]. With our formalism we have $\vec{v}^T M^T M \vec{v} - \lambda(\vec{v}^T \vec{v} - 1)$, hence $2M^T M \vec{v} - 2\lambda \vec{v} = 0$, and then $M^T M \vec{v} = \lambda \vec{v}$. This is an eigenvalue equation, which can be solved numerically. More

eigenvectors are sought through a similar procedure, with the additional constraints that the eigenvectors must be orthogonal to each other. Since the eigenvalues are a measurement of the sum of the squared projections of the original data vectors on the new normalized vectors, and since we assume to have set as a covariance matrix $M^T M$, the eigenvalues are a measurements of the amount of variance carried in each new direction. For example, in a plane we can imagine a set of almost aligned points; their projections in the original axes may be nearly equal if they are not aligned preferentially with anyone of the two axes of the two original frame. In a physical context we may think of two variables that are highly correlated. We can maximize the projections along one axis by simply operating a rotation of the reference frame. A linear combination of the two original variables (or vectors) will now constitute the one vector that is needed to account for the variance of the data. A key aspect of the power of the PCA emerges from this simple example: a problem originally treated in two dimensions was inherently one-dimensional i.e., a PCA can restore a problem with a very large set of variables to its intrinsic dimensionality.

2.3 The Original Eigenvectors by Boroson & Green

The first important application of PCA to the interpretation of quasar spectra was done in the early 1990s on a sample of 87 objects of the PG survey at $z < 0.5$ [22]. T. Boroson & R. Green measured the most prominent emission features in the $H\beta$ spectral region, and found that most of the variance was related to two sets of correlations, the first being an anti-correlation between the prominence of $[OIII]\lambda\lambda 4959,5007$ and optical FeII emission ($FeII_{opt}$). The “eigenvector 1” has been later found in a number of much larger samples [21, 88, 122, 229, 230, 285], and with spectral parameters describing phenomenologies as apparently distant as the X-ray continuum continuum shape and the radial velocity shift of high ionization emission lines. Even if many pieces of the eigenvector analysis had been hinted at by previous workers [18, 138, 263], the “eigenvector 1” provided, for the first time, a powerful systematic description of quasar spectral diversity. The second eigenvector involved the optical luminosity and the strength of the high ionization line (HIL) $HeII\lambda 4686$. This second eigenvector had been also found by previous workers, and is basically the “Baldwin effect” (§8.4).

2.4 The Optical Eigenvector 1 Plane

It is remarkable that the spectral diversity of quasars can be reduced (if we exclude any luminosity dependence) to just two variables. The diversity and correlation of broad line AGNs are clearly shown by their distribution in the so-called “Eigenvector 1 (E1) optical plane,” defined by the FWHM of the $H\beta$ broad component, $FWHM(H\beta_{BC})$, and by the equivalent width ratio between the Fe II blended emission at $\lambda 4570$ and the $H\beta$ broad component, $R_{FeII} = W(FeII \lambda 4570)/W(H\beta_{BC})$ [21, 22, 229]. The anti-correlation between $FWHM(H\beta_{BC})$ and R_{FeII} provides perhaps a superior description of E1 than the original one, since it involves parameters related to the broad lines only ($[OIII]\lambda\lambda 4959,5007$ are narrow lines affected by radio loudness; [230]). The modest spread of data points drawn

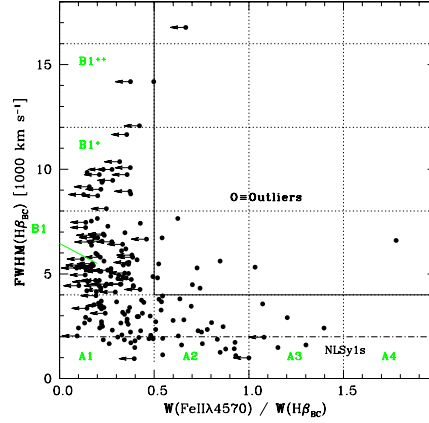


Figure 2: The Optical Plane of the eigenvector 1 of type-1 AGNs; abscissa is the equivalent width ratio between FeII $\lambda 4570$ and $H\beta_{BC}$, ordinate is FWHM of $H\beta_{BC}$ in km s^{-1} . The plane has been subdivided in spectral type according to Ref. [230]. The dot-dashed line identifies Narrow Line Seyfert 1s, defined by the condition $\text{FWHM}(H\beta_{BC}) < 2000 \text{ km s}^{-1}$. In the outlier regions, very few genuine sources (i.e., excluding those that are borderline because of errors) are found. Data are from Marziani et al. [140]

from a sample of more than 200 type-1 AGNs allow the definition of typical spectral types covering a narrow range in $\text{FWHM}(H\beta_{BC})$ and R_{FeII} [230]. We set $\Delta R_{\text{Fe}} = 0.5$, and, for $\text{FWHM}(H\beta_{BC}) \lesssim 4000 \text{ km s}^{-1}$, we define spectral type A1, A2, A3 in order of increasing R_{FeII} (see Fig. 2; FeII emitters are considered strong if $R_{\text{FeII}} \gtrsim 1$; extreme if $R_{\text{FeII}} \gtrsim 1.5$). Sources with $\text{FWHM}(H\beta_{BC}) \gtrsim 4000 \text{ km s}^{-1}$ very rarely show $R_{\text{Fe}} \gtrsim 0.5$. If $R_{\text{Fe}} \lesssim 0.5$, we define a second sequence of increasing $\text{FWHM}(H\beta)$ (A1, B1, B1⁺ . . .) with $\Delta \text{FWHM}(H\beta) \approx 4000 \text{ km s}^{-1}$. The spectral types are easy to identify observationally, even from a visual inspection of the optical spectrum (Fig. 3) and most of them may have a direct physical meaning (§ 2.6, 2.7, §7). $\text{FWHM}(H\beta_{BC}) \approx 4000 \text{ km s}^{-1}$ represents a notable limit. It separates two groups of AGNs, Population A and B [229] whose different properties are most likely related to structural differences in the Broad Line Region (BLR; see §3).

2.5 Eigenvector 1 Measurements

Quoting Peterson et al. [179], we can say that *accurate line-width measurement depends critically on avoiding contaminating features, in particular the narrow components of the emission lines*. Fig. 4 illustrates the typical analysis and measurement procedure applied to optical and UV data, in the $H\beta$ (left panel) and $\text{CIV} \lambda 1549$ (right panel) spectral region. Two

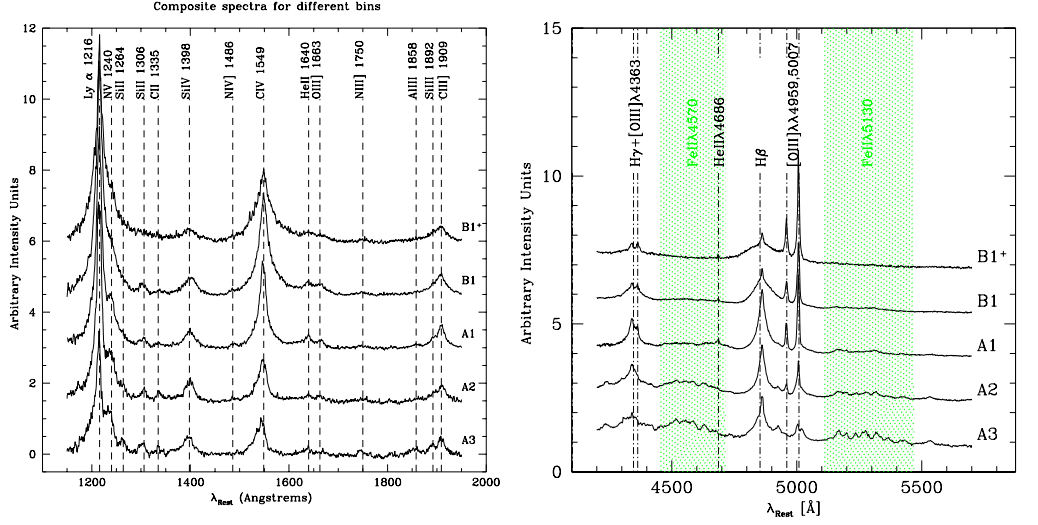


Figure 3: Spectral diversity organized along the E1 sequence for UV (left panel) and optical (right panel) spectra, for the spectral types defined according to Sulentic et al. [230]. Prominent blends of FeII emission are shaded.

sources – one representative of Pop. A and the other of Pop. B – are shown. After continuum subtraction, FeII can be measured through a template FeII spectrum. Measurement of FeII λ 4570 (i.e., FeII emission integrated over the wavelength range 4434–4684 Å) parameters like flux and width are accomplished by constructing an array of template spectra within reasonable limits of scaling and broadening factors [22, 138, 140], starting from a template (the I Zw 1 FeII spectrum). One then obtains the best scaling and broadening factor by subtracting the templates and by identifying the one template that minimizes the sum of the least-square residuals in the range 4450–4600 Å. In principle, FeII and continuum should be fit simultaneously in an automatized way [75], especially if FeII is very strong. A similar procedure [59, 58, 121, 138, 258] is applied to the CIV λ 1549 spectrum using an FeII_{UV} emission template [138, 258, 276]. While the procedure works remarkably well in the optical and in the UV around 1600 Å, some caution is needed in the UV between 2000 Å and 3000 Å since FeII emission around MgII λ 2800 can be strong and different from source to source [104].

We usually isolate the contribution of H β _{NC}, [OIII] λ 4959, 5007, and of broad HeII λ 4686 before we apply a high-order spline fit to produce a model-independent “description” of H β _{BC} which minimizes the effects of noise (the thick lines in the side panels of Fig. 4; [140]). Measurements of FWHM(H β _{BC}) are one of the basis of black hole mass estimates, so that it is important to provide a reliable recipe that leads to accurate results. Subtraction of a narrow-line component H β _{NC} is best done according to the following criteria [140]: (1) if a clear inflection is seen, the subtraction is trivial. This is the case of most sources (see the example of NGC 3783 in Fig. 4); (2) in the case where an inflec-

tion is not seen, we subtracted a Gaussian profile under the condition that $\text{FWHM}(\text{H}\beta_{\text{NC}}) \approx \text{FWHM}([\text{OIII}]\lambda\lambda 4959, 5007)$. It is important to stress that this last condition is not always applicable; (3) for several Pop. A sources (e.g., “Narrow Line Seyfert 1s” (NLSy1s) like Ton 28 shown in Fig. 4) with typically Lorentzian profiles and $\text{FWHM} \lesssim 4000 \text{ km s}^{-1}$ (§2.8), the inflection is not observed. Such sources are “blue outliers” i.e., objects for which the recessional velocity measured on $[\text{OIII}]\lambda\lambda 4959, 5007$ is lower than that of $\text{H}\beta_{\text{NC}}$ by more than 250 km s^{-1} [288]. Subtraction of a significant narrow component in many of these sources would imply $\text{H}\beta_{\text{NC}}$ stronger than or comparable to $[\text{OIII}]\lambda 5007$, which is not consistent with other forbidden line ratios [158]. Typically, $\text{H}\beta_{\text{NC}}$ is 1/10 the strength of $[\text{OIII}]\lambda 5007$. In the outliers, any $\text{H}\beta_{\text{NC}}$ would be appreciably displaced along the $\text{H}\beta_{\text{BC}}$ profile. However, since $W([\text{OIII}]\lambda 5007) \lesssim 2.5 \text{ \AA}$, the $\text{H}\beta_{\text{NC}}$ becomes too weak to be detected (very high resolution spectra are needed; it is detected for I Zw 1 [255], and references therein). This argues against the subtraction of a strong $\text{H}\beta_{\text{NC}}$ in blue outliers if high-resolution does not resolve a low-ionization $\text{H}\beta_{\text{NC}}$ [255]. If this recipe is applied, $\text{FWHM}(\text{H}\beta_{\text{BC}})$ measurements with an accuracy of $\pm 10\%$ at a 2σ confidence level are possible for the wide majority of “good” spectra. We customarily isolate a narrow-component contribution also to $\text{CIV}\lambda 1549$ before the $\text{CIV}\lambda 1549_{\text{BC}}$ is fit. Since the presence of significant $\text{CIV}\lambda 1549_{\text{NC}}$ has been debated, we discuss the issue in physical terms in §4.7.1.

2.6 Eigenvector 1 Correlates

2.6.1 FeII

The emission spectrum of FeII in AGNs spans a wide wavelength range from the UV to the IR. It affects not only line intensity measurements of other ions but the continuum determination as well. In case of the strong FeII_{UV} , the emission produces a pseudo-continuum that extends to wavelengths as short as 1000 \AA , and is especially strong in the near UV between 2000 and 3000 \AA (Fig. 1; [138, 250, 276]). A convenient subdivision of FeII emission may be as follows: (1) FeII_{UV} , between 2000 and 3000 \AA [104, 250]; (2) near FeII_{UV} between 3000 and 3500 \AA ; (3) $\text{FeII } \lambda 4570$, whose values are probably the most frequently reported FeII_{opt} measurements [22, 140]. Under the assumption that the I Zw 1 spectrum is a good representation of optical FeII emission, it is $\text{FeII } \lambda 4570 / \text{FeII}_{\text{opt}} \approx 3.3$ [138]; (4) $\text{FeII } \lambda 5250$ i.e., the emission blend on the red side of $\text{H}\beta$ (see Figs. 1 and 3).

FeII emission is still rather poorly understood, even if several recent papers have made significant advances after a decade-long standstill (see Ref. [229] for a bibliography before late 1999). An extremely complex energy level structure of FeII makes it very difficult to obtain all the experimental transition probabilities and therefore calculate line intensities ([6, 221, 252], and references therein). Although $Z \gg Z_{\odot}$ does not seem anymore a requirement for explaining very large $\text{FeII}_{\text{UV}} / \text{MgII}\lambda 2800$ ratios [250], there is still no general consensus on the excitation mechanism. There are two lines of thought: Fe^+ is mainly produced by photoionization; collisional excitation and florescence produce the observed strength and multiplet ratio. A recent paper [249] accounts for the observed $\text{FeII}_{\text{UV}} / \text{FeII}_{\text{opt}}$ and $\text{FeII}_{\text{UV}} / \text{MgII}\lambda 2800$ intensity ratios. Large electron density n_e (UV multiplets are fa-

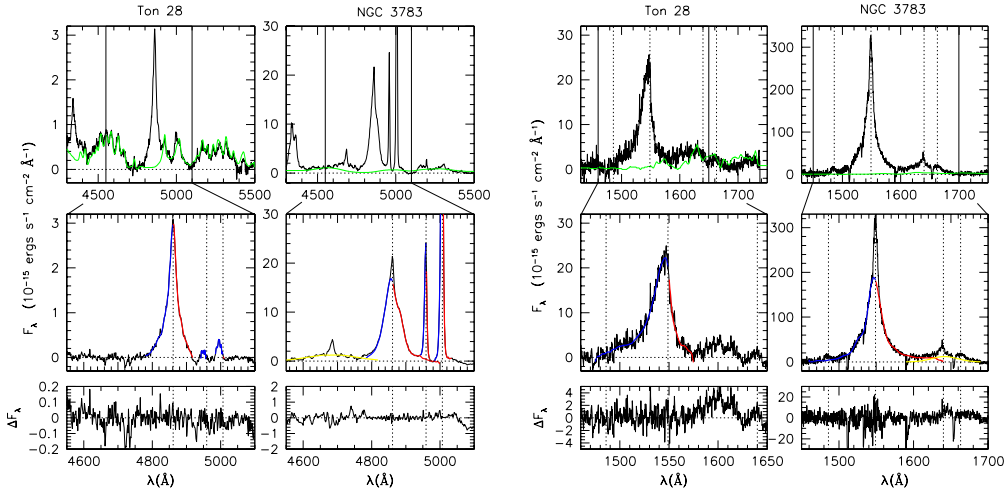


Figure 4: Line profile analysis for two sources in widely different positions along the E1 sequence (Ton 28, a NLSy1, and NGC 783), for $H\beta$ (left panels) and $CIV\lambda 1549$ (right panels). The upper panel shows the continuum subtracted spectra, with the FeII contribution highlighted. The middle panel emphasizes the $H\beta_{BC}$ profile as well as the $HeII\lambda 4686$ line. Note that the $[OIII]\lambda\lambda 4959, 5007$ lines of Ton 28 are significantly blueshifted with respect to the rest frame; Ton 28 is a “blue outlier”.

vored because of the increase in the upper level population) and moderate micro-turbulence (broadening $\sim 10 \text{ km s}^{-1}$) can account for the combination of important diagnostics such as the $FeII_{UV}/MgII\lambda 2800$, and $FeII_{UV}/FeII_{opt}$ intensity ratio [250]. However, models based on photoionization are not void of difficulties: a recent work indicates that photoionized BLR gas cannot produce both the observed shape and observed equivalent width of the 2200–2800 Å $FeII_{UV}$ bump unless there is considerable velocity structure corresponding to a microturbulent velocity parameter $v_{turb} \sim 100 \text{ km s}^{-1}$, which strongly favor fluorescent processes [6]. A second line of thought ([43, 255], and references therein) suggest that modelling the spectrum of the BLR requires a non radiative heating mechanism which increases the temperature in the excited HI region, thus providing the necessary additional excitation of the FeII lines [107]. The specificity of such a medium compared with a photoionized medium is its extremely low degree of ionization. The emission spectrum is made exclusively of low ionization lines (LILs) like FeII, Balmer lines and $MgII\lambda 2800$ for the electron density n_e typical of the BLR. The photoionization models require very high ionizing photon fluxes $\sim 10^{20} - 10^{21} \text{ cm}^{-2}\text{s}^{-1}$ to explain very large $FeII_{UV}/MgII\lambda 2800$ ratios, while collisionally heated media require a shielding mechanism to hide the emitting regions from the strong AGN continuum. On the basis of our current understanding of the line emitting region structure (§3), it is not clear where this shielded medium could be [43, 6].

Even if the poor understanding of FeII processes hampers the use of FeII emission as a diagnostics, there are several important constraints related to E1:

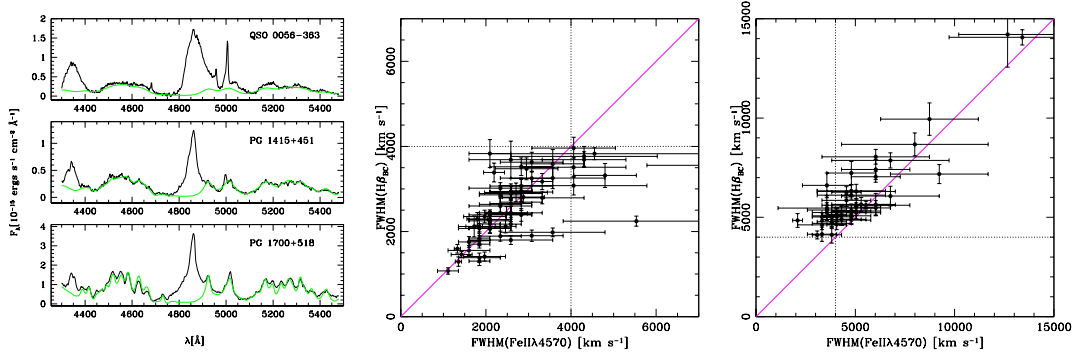


Figure 5: The left panel shows three examples with widely different $\text{FWHM}(\text{FeII } \lambda 4570)$; it is shown that the I Zw 1 template, opportunely scaled and broadened, provides a good fit to all three sources (it provides a satisfactory reproduction to FeII_{opt} of almost all sources [140]). The middle and right panel show the correlation between $\text{FWHM}(\text{H}\beta_{\text{BC}})$ and $\text{FWHM}(\text{FeII } \lambda 4570)$, for $\text{FWHM}(\text{H}\beta_{\text{BC}}) \leq 4000 \text{ km s}^{-1}$ and $\text{FWHM}(\text{H}\beta_{\text{BC}}) > 4000 \text{ km s}^{-1}$ respectively.

- $\text{FeII } \lambda 4570$ emission is well reproduced, in a sample of 300 AGNs [140, 143] by a scaled and broadened I Zw 1 FeII_{opt} template. All sources did not show any *strong* deviation from the template within the limits imposed by S/N and resolution. Measurements of FeII width and strength are intrinsically difficult. Non optimal intrinsic width, spectral coverage, and S/N imply that only an upper limit to the equivalent width can be measured for faint FeII sources (see Fig. 2);
- Fig. 5 shows that the template method is able to reproduce FeII in cases of widely different width and strength. At zero order, Fig. 5 confirms that FeII and $\text{H}\beta_{\text{BC}}$ are approximately of the same width, suggesting a common origin for these two LILs and confirming that R_{FeII} is a meaningful parameter. There is however a difference: while for $\text{FWHM}(\text{H}\beta_{\text{BC}}) \lesssim 4000 \text{ km s}^{-1}$ we have $\text{FWHM}(\text{H}\beta_{\text{BC}}) \approx \text{FWHM}(\text{FeII } \lambda 4570)$ in a rigorous statistical sense, a sign test suggests that $\text{FWHM}(\text{H}\beta_{\text{BC}}) \gtrsim \text{FWHM}(\text{FeII } \lambda 4570)$ if $\text{FWHM}(\text{H}\beta_{\text{BC}}) \gtrsim 4000 \text{ km s}^{-1}$ [142];
- the $\text{FeII}_{\text{UV}}/\text{MgII}\lambda 2800$ ratio seems to be E1 dependent, in the sense that sources with the narrowest $\text{FWHM}(\text{H}\beta_{\text{BC}})$ [140] show the largest values of $\text{FeII}_{\text{UV}}/\text{MgII}\lambda 2800$ [104, 121]. The $\text{FeII}_{\text{UV}}/\text{MgII}\lambda 2800$ ratio increase along the E1 sequence may imply higher iron abundance but is also consistent with an increase in n_e , if density changes from $n_e \lesssim 10^{10} \text{ cm}^{-3}$ to $n_e \sim 10^{11} \text{ cm}^{-3}$ [250]. Largest $\text{FeII}_{\text{UV}}/\text{MgII}\lambda 2800$ (≈ 10) ratios require $n_e \sim 10^{11} \text{ cm}^{-3}$. Higher density is supported by several lines of evidence ([4, 139]; §2.8).

2.6.2 Prominence of [OIII] $\lambda\lambda$ 4959,5007

The prominence of [OIII] $\lambda\lambda$ 4959,5007 is one of the most basic correlates along E1, especially if the parameter actually measured is the peak height over continuum [21, 22]. Although not customary, this parameter yields a better correlation since profiles tend to broaden at low intensity [288], making $W([OIII]\lambda\lambda 4959,5007)$ a worse correlate. Emission of [OIII] $\lambda\lambda$ 4959,5007 is not straightforward to interpret. If a sample covers low- z sources and spans a large z range, [OIII] $\lambda\lambda$ 4959,5007 measures are prone to aperture effects since the [OIII] $\lambda\lambda$ 4959,5007 emission morphology can be anisotropic [98]. Resolved “narrow line regions” (NLRs i.e., where [OIII] $\lambda\lambda$ 4959,5007 is produced) reveal that line emission is not only anisotropic but also strongly influenced by radio jets, in nearby RQ Seyfert nuclei and in BLRG alike [15, 36, 70, 271]. Not surprisingly, the EW of [OIII] $\lambda\lambda$ 4959,5007 is in RL than in RQ sources of the same optical spectral type [125, 21, 143]. In addition, [OIII] $\lambda\lambda$ 4959,5007 profiles can be strongly asymmetric with a predominance of blue-ward asymmetries ([271], and references therein). In the E1 context we find that large $W([OIII]\lambda\lambda 4959,5007)$ sources can have a blue-ward asymmetric wing; low $W([OIII]\lambda\lambda 4959,5007)$ sources (located in the lower left part of the optical E1 diagram; [288]) have emission entirely ascribable to a semi-broad, blueshifted feature that may resemble the blueward wing observed in stronger [OIII] $\lambda\lambda$ 4959,5007 emitters.

2.7 Eigenvector 1 Extremes

Narrow Line Seyfert 1s NLSy1s have been recognized as a distinct type of Seyfert nuclei since 1985 [172]. The defining criterion is that the width of the Balmer lines be less than 2000 km s^{-1} . The [OIII] λ 5007/ $H\beta$ ratio (but $H\beta$ is not necessarily $H\beta_{NC}$!) is often smaller than 3 [46, 215]. NLSy1s usually (but not always) show rather strong $FeII_{opt}$ emission. Their soft X-ray spectra are very steep [248, 263] and variable (e.g., [90, 241]). The original definition is not void of difficulty, since: (1) a sharp discontinuity in many properties of type-1 sources is seen at $FWHM(H\beta_{BC}) \approx 4000 \text{ km s}^{-1}$, and not at $FWHM(H\beta_{BC}) \approx 2000 \text{ km s}^{-1}$ (§2.6). In other words, in the range $2000 \text{ km s}^{-1} \lesssim FWHM(H\beta_{BC}) \lesssim 4000 \text{ km s}^{-1}$ sources show properties consistent with the ones of NLSy1, although less extreme. (2) Sources with $R_{FeII} \lesssim 0.5$ (spectral type A1; [230]) may not be true NLSy1s since they often show prominent [OIII] $\lambda\lambda$ 4959,5007, and their $H\beta_{BC}$ profiles can be different from the typical NLSy1 and bin A2 and A3 profiles; several sources are core-dominated RL sources and some belong to the second extremal type mentioned in §1.2. With these caveats in mind, NLSy1s seem to be drivers of the E1 correlations since they show and minimum $FWHM(H\beta_{BC})$ and may have extreme R_{FeII} in the “main sequence” of the optical E1 plane [229]. In the context of E1 they are interpreted as young or rejuvenated gas-rich objects with low black holes mass and high accreting rate [46, 88, 119, 144, 180].

BAL QSOs High- z and low- z BAL QSOs share some of the properties of the extreme Pop. A sources in the E1 optical diagram: weaker $CIV\lambda 1549_{BC}$ in emission [97, 242]; stronger $FeII_{UV}$ and $AlIII\lambda 1808$ [261], as well as stronger $NV\lambda 1240$. BAL QSOs occur

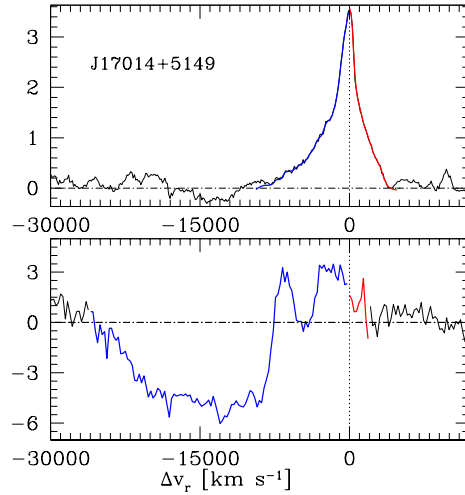


Figure 6: Inter-profile $H\beta$ and $CIV\lambda 1549$ comparison for the prototypical BAL QSO PG 1700+518. The profiles are shown here after continuum and FeII subtraction. Note that the $CIV\lambda 1549$ emission component is almost fully blueshifted with respect to the quasar rest frame.

with a frequency of $\approx 15\%$ with respect to all quasars [196]; the fraction of radio-loud BAL quasars may be consistent with the fraction of radio-loud ordinary quasars [239]. The “Balnicity” Index [269] distribution rises with decreasing index values. This suggests that the fraction of quasars with intrinsic outflows may be significantly underestimated [196]. Several high- z BAL QSOs have extremely strong FeII and very weak $[OIII]\lambda\lambda 4959, 5007$, extending the inverse relationship found for low- z QSOs and typical of Pop. A [287]. An important information that is still missing for most high- z BAL sources is a reliable estimate of the systemic redshift [117]. Without this information, the interpretation of the $CIV\lambda 1549$ absorption/emission profile is rather ambiguous. Identification of low- z BAL sources had to await space-based UV observatories [23, 225, 243], and only a handful of sources is known to-date. Classical BAL sources with Balnicity Index $\gg 0 \text{ km s}^{-1}$ at low and high z for which the rest frame can be reasonably set from narrow lines show an almost fully blueshifted emission component of $CIV\lambda 1549$ in addition to a fully blueshifted absorption ([225]; Fig. 6). Most low- z BAL AGNs with terminal wind velocities in the range $\approx 20000\text{-}30000 \text{ km s}^{-1}$ are either outliers or are located along the upper envelope of the E1 “main sequence” for Pop. A sources. Most revealing are the cases of Mkn 231 and IRAS 07598+6508, which are basically the only 2 outliers in a sample of ~ 300 low- z AGNs. The sources show $FWHM(H\beta_{BC})$ significantly larger than $FWHM(FeII_{opt})$. The difference is due to a strong blue-ward asymmetry visible in the $H\beta_{BC}$ profile. The $H\beta_{BC}$ profile can be interpreted as due to a narrower component with $FWHM \approx FWHM(FeII_{opt})$, and to a completely blueshifted feature, most probably associated to an high ionization

outflow emitting most of HILs like $\text{CIV}\lambda 1549$. If this effect is taken into account, and $\text{FWHM}(\text{FeII}_{\text{opt}})$ instead of $\text{FWHM}(\text{H}\beta_{\text{BC}})$ is used, Mkn 231 and IRAS 07598+6508 move into the “main sequence” optical E1 diagram to become extreme (in terms of R_{FeII}) Pop. A sources.

Radio Quiet & Radio Loud Quasars $\text{FWHM}(\text{H}\beta_{\text{BC}})$ in RL sources are at least twice as large as the RQ majority [229]. The average broad FeII $\lambda 4570$ emission line strength is also about half that for RQ sources [22, 106, 138]. Fig. 7 shows that the Fanaroff-Riley II (i.e., lobe-dominated, LD) “parent population” of relatively un-boosted RL sources (median radio/optical flux ratio $R_K \sim 500$) shows the most restricted occupation. The Doppler boosted core-dominated (CD) RL sources (median $R_K \sim 1000$) lie towards smaller $\text{FWHM}(\text{H}\beta_{\text{BC}})$ and stronger FeII in E1 as expected if the lines arise in an accretion disk.

2.8 Additional E1 Correlates

$\text{H}\beta_{\text{BC}}$ Profile Shape Median spectra of the $\text{H}\beta_{\text{BC}}$ profile were extracted for each spectral type (Fig. 2) after FeII_{opt} and continuum subtraction in a sample of ~ 200 AGNs [140, 230]. The median $\text{H}\beta_{\text{BC}}$ profiles in spectral types A are almost symmetric, with a slight blueward asymmetry in bin A2 (see Fig. 2 for the definition of the spectral types). The blue asymmetry becomes visually apparent in bin A3 which contains sources that are extreme in many ways. The median profiles of Pop. B sources are very redward asymmetric, with the strongest asymmetry in the (few) bin B1 sources. The $\text{H}\beta_{\text{BC}}$ profile in NLSy1 and Pop. A sources is well fit by a Lorentz function [254]. The best fit to $\text{H}\beta_{\text{BC}}$ bin B1 and B1^+ profiles is achieved through the sum of two Gaussians: (1) an unshifted Gaussian core ($\text{FWHM}(\text{H}\beta_{\text{BC}}) \sim 5000 \text{ km s}^{-1}$) and (2) a broader redshifted Gaussian base with $\text{FWHM} \sim 10000 \text{ km s}^{-1}$ [29]. We remark that a Double Gaussian fit to $\text{H}\beta_{\text{BC}}$ in Pop. B sources is a formal result. The two components have a physical justification if, for the generality of AGNs, the broader one can be ascribed to gas that lies closest to the continuum source in an optically thin (to the HI ionizing continuum) region with large covering factor $f_c \rightarrow 1$ [29, 30, 136, 214].

$[\text{OIII}]\lambda\lambda 4959, 5007$ blueshifts The narrow lines of $[\text{OIII}]\lambda\lambda 4959, 5007$ usually provide a reliable measure of the systemic, or rest-frame, quasar velocity. However, several observations indicate that the NLSy1 galaxy prototype I Zw 1 shows an $[\text{OIII}]\lambda\lambda 4959, 5007$ blueshift of $\approx -500 \text{ km s}^{-1}$ relative to other rest-frame measures [24, 138], with a second component at $\approx -1500 \text{ km s}^{-1}$ (see references in Ref. [255]). I Zw 1 is not alone. It is possible to identify sources with $[\text{OIII}]\lambda\lambda 4959, 5007 \Delta v_r \gtrsim -300 \text{ km s}^{-1}$ with respect to $\text{H}\beta_{\text{NC}}$. Such large shifts are unlikely to be due to measurement errors [288]. The two known largest blueshift after I Zw 1 reach $\Delta v_r \sim -1000 \text{ km s}^{-1}$ [2]. Since these sources are apparently rather rare (but not unique! [89, 91, 143]), and since they seem to lie out of a continuous shift distribution, they have been dubbed “blue outliers”. The distribution of blue outliers in the E1 optical plane is different from that of the general AGN

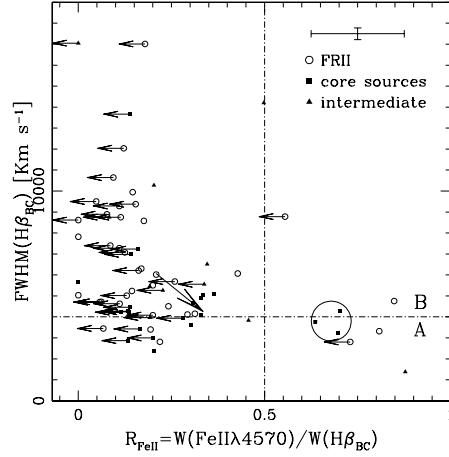


Figure 7: Distribution of RL sources in the optical plane of the eigenvector 1 of type-1 AGNs; abscissa is the equivalent width ratio between FeII $\lambda 4570$ and $H\beta_{BC}$, ordinate is FWHM of $H\beta_{BC}$ in km s^{-1} . The big arrow indicates displacement between the median R_{FeII} and FWHM($H\beta_{BC}$) values from lobed and pure core RL sources. The circle identifies CD sources that genuinely have $R_{\text{FeII}} \gtrsim 0.5$ [234]; other sources at $R_{\text{FeII}} \gtrsim 0.5$ are strongly affected by measurement errors.

population [288]. The blue outliers occupy the lower right part of the diagram and are exclusively Pop. A/NLSy1 nuclei [289]. Low $W([\text{OIII}]\lambda\lambda 4959, 5007)$ may show only a blue-shifted component as if only the asymmetric part of the profile observed in stronger sources is being emitted. It is relatively straightforward to interpret the large blueshift and the profile of the $[\text{OIII}]\lambda\lambda 4959, 5007$ lines as the result of an outflow [2, 288], and the low $W([\text{OIII}]\lambda\lambda 4959, 5007)$ as a signature of a compact NLR [255, 288].

High Ionization Lines The peak shift of the prototypical HIL $\text{CIV}\lambda 1549$ is an important E1 correlate in the sense that large shifts are shown only for $\text{FWHM}(H\beta_{BC}) \lesssim 4000 \text{ km s}^{-1}$ [4, 138, 231] at low z . $W(\text{CIV}\lambda 1549)$ decreases along the E1 sequence from sources with large $\text{FWHM}(H\beta_{BC})$ and low R_{FeII} (typical $W(\text{CIV}\lambda 1549_{BC}) \sim 100 \div 200 \text{ \AA}$) to the most extreme NLSy1s (typical $W(\text{CIV}\lambda 1549_{BC}) \lesssim 50 \text{ \AA}$; [4, 138, 203, 231]).

Ionization Level/Electron Density A decrease in equivalent width of $\text{CIV}\lambda 1549$ and $H\beta_{BC}$ along with an increase in prominence of FeII $\lambda 4570$ in the E1 sequence toward NLSy1 sources suggest a systematic decrease in ionization level from RQ Pop. B to Pop. A [139]. The behavior of $W(\text{CIV}\lambda 1549)$ and $W(H\beta_{BC})$, and of the diagnostic ratios $\text{SiIII}\lambda 1892 / \text{CIII}\lambda 1909$ and $\text{AlIII}\lambda 1808 / \text{CIII}\lambda 1909$ can be understood in terms of a decrease in ionization parameter U (defined as the ratio between the ionizing photon flux and the electron density n_e) and an increase in n_e from $\log U \sim -1$, $\log n_e \sim 9.5$,

to $\log U \sim -2 \div -2.5$, $\log n_e \sim 10.5 \div 11$ [4, 115, 139]. Notably, the diagnostic ratios indicate that $\log n_e \sim 10.5 \div 11$ towards the NLSy1 domain (see also Ref. [255] for I Zw 1).

X-ray Continuum The soft (energy $\lesssim 2\text{-}3$ KeV) X-ray excess [45, 272] is perhaps the most distinctive X-ray feature that differentiate sources along E1 [263, 229]. The nature of the soft X-ray excess is still debated, although direct thermal emission from the accretion disk seems to be ruled out on the basis of the very high temperature derived for this optically thick component [186]. Even the newest X-ray data cannot constraint the current models [28, 85]. In the context of E1 several recent studies (including XMM-Newton observations; [186, 189]) reveal systematic differences in the X-ray properties of RL and RQ quasars. XMM observations [186] confirm a previously reported anti-correlation between soft and hard photon indices and $\text{FWHM}(\text{H}\beta_{\text{BC}})$ [195, 263]. The soft X-ray spectral index correlates with the hard-X ray spectral shape, in the sense that NLSy1 and Pop. A sources have a steeper spectral shape [129].

UV Continuum Inferences on UV/FUV continuum shape are complicated by the lack of data at low z before the advent of HST and FUSE, as well as by the possibility of strong extinction. A breakthrough occurred with the discovery in the spectrum of 3C273 of an optical-UV feature called the “Big Blue Bump”, corresponding to an important fraction of the bolometric luminosity. Some soft X-ray selected AGNs are NLSy1 galaxies with an enhanced big blue bump emission component relative to the underlying continuum making the optical continuum blue and the soft X-ray spectrum steep [90]. On the other hand, several recent works indicate that NLSy1s have a redder continuum than the rest of type-1 AGNs [52, 46, 266]. After correcting with an extinction curve obtained from ~ 1000 AGNs, it seems that radio-quiet AGNs have very similar intrinsic UV-to-optical continuum shape over several orders of magnitude in luminosity, and that that radio-loud and radio-quiet AGNs probably share the same underlying continuum shape [83]. A recent investigation of ultraviolet-to-optical Spectral Energy Distribution (SED) of 17 AGNs used quasi-simultaneous spectrophotometry spanning $900\text{-}9000$ Å (rest frame) with FUSE, HST and the 2.1-meter telescope at KPNO to study the big blue bump. Most objects exhibit a spectral break around 1100 Å, with a slope slightly steeper for RL sources [65, 212, 247, 290], but otherwise there is no obvious trend which may be related to the source location in the E1 sequence (apart from extinction).

FIR excess Several quasars show an SED with an extremely strong FIR excess [20, 26, 202, 225]. The strong excess can be due, at least in part, to the contribution of circumnuclear starburst, as in the case of Mkn 231 [57], or to reprocessed radiation from a dusty torus encircling the accretion disk and the BLR. NLSy1s and extra-strong FeII sources are known to be found often among sources detected by the *Infra-Red Astronomical Satellite* [133, 154], although it is as yet unclear how frequent is a FIR bump among NLSy1s [215].

Bolometric Correction It is not easy to obtain L_{bol} for individual quasars because they emit significant power over a large part of the electromagnetic spectrum, most notably in the FUV and in the FIR. Bolometric correction factors are found to be $L_{\text{bol}} \approx 9 \div 13 \lambda L_{\lambda}$ ergs s^{-1} for $\lambda \approx 5400 \text{ \AA}$, with possible deviations for single sources of amplitude $\pm 50\%$ [65, 212, 281]. A bolometric relationship $L_{\text{bol}} = 9 \div 10 \lambda L_{\lambda}$ ergs s^{-1} has been often adopted [41, 108, 143, 262, 281]. Recent work based on good coverage of the UV, FUV and X but still poor sampling of the IR SED confirms that the assumption $L = 13 \lambda L_{\lambda}$ ergs s^{-1} at 5400 \AA is a fairly good approximation [212]. Again, scatter is pretty large ($\pm 50\%$). To test any dependence of the bolometric correction along E1, we analyzed 44 sources that share accurate $\text{H}\beta_{\text{BC}}$ measurements [140] and SEDs constructed from archival data [281]. Comparison of L_{bol} values computed from the SED and from the bolometric correction showed no significant systematic difference: the average $\Delta \log L_{\text{bol}}$ is ≈ -0.06 for all 44 sources, with a standard deviation $\sigma \approx 0.24$. Similar results hold if RQ Pop. A sources and RL AGNs are considered separately. It is worth noting that the scatter is due to a minority of badly behaving data points ($\approx 20\%$). If they are removed, the standard deviation becomes $\sigma \approx 0.1$ in all cases, with systematic differences always $\lesssim 0.05$. Although big blue bump studies show that there may be a gross uniformity as far as the FUV is concerned, the difficulty to assess prominence and inherence of any FIR bump as well as the still uncertain shape in the EUV warrant caution before claims of accuracy better than $\pm 50\%$ can be believed for the bolometric correction of individual objects. It is also important to stress that sources which are RL CD could add an appreciable scatter to an average SED, since their continuum may be strongly affected by relativistic beaming. RL CD sources should be considered on an individual basis and not included in averages.

X-ray Variability A common phenomenon observed in AGNs is variability (for a review see e.g., Ref. [244]). The most vigorous variability observed is that of the X-rays [157]. Giant-amplitude X-ray variability by more than a factor of 15 has been found in NLSy1 galaxies. The most extreme one is IRAS13224-3809 which raised by a factor of about 57 in just two days [19]. This giant variability is persistent [79, 286]. Examination of X-ray properties across the Seyfert population reveals an anti-correlation between variability amplitude and $\text{FWHM}(\text{H}\beta_{\text{BC}})$ [91, 241].

Optical Variability Optical variability has been established as an identifying property of type-1 AGNs for more than three decades. Typically these objects show continuum variations by 1-2 magnitudes with timescales ranging from days to years [185, 267]. Broad emission lines have also been found to vary. Emission line variations lag the continuum variations with delays ranging from a few days to months [51, 183]. The conclusion of an optical photometric study on six NLSy1s is that, as a class, there is no evidence that NLSy1s behave any differently than broader-lined Seyfert 1s [110]. However, an earlier study [268] conducted on a large sample (23 AGNs) found some evidence that AGNs with the strongest FeII emission lines were less likely to show strong optical variability. In the E1 context, an unpublished analysis of a survey of PG quasars [86] suggests that strong

optical variability $\Delta m \sim 0.5$ is not present among sources with $\text{FWHM}(\text{H}\beta_{\text{BC}}) \lesssim 4000 \text{ km s}^{-1}$, and $R_{\text{FeII}} \gtrsim 0.5$; it seems to be frequent for $\text{FWHM}(\text{H}\beta_{\text{BC}}) \gtrsim 4000 \text{ km s}^{-1}$, and, interestingly enough, for sources with $\text{FWHM}(\text{H}\beta_{\text{BC}}) \lesssim 4000 \text{ km s}^{-1}$ and $R_{\text{FeII}} \lesssim 0.5$.

Summing up, along the E1 sequence we see extreme X-ray variability in correspondence of the high R_{FeII} , low $\text{FWHM}(\text{H}\beta_{\text{BC}})$ end; optical variability, on the other hand, seems to follow the opposite trend: to be modest or even undetected in NLSy1s sources, and to be of relatively large amplitude for some sources with broader lines.

Table 1: Main Trends Along the E1 Sequence

	Large R_{FeII} Small $\text{FWHM}(\text{H}\beta_{\text{BC}})$	Low R_{FeII} Large $\text{FWHM}(\text{H}\beta_{\text{BC}})$
$\text{W}(\text{H}\beta_{\text{BC}})$	low	large
$\text{H}\beta_{\text{BC}}$ shape	Lorentzian	redward asymmetric; double Gaussian
$\text{CIV}\lambda 1549$ shift	large blueshift	no shift
$\text{W}(\text{CIV}\lambda 1549)$	low	high
$\text{CIV}\lambda 1549_{\text{NC}}$	no	may be prominent
$\text{W}([\text{OIII}]\lambda\lambda 4959, 5007)$	lower	larger
$[\text{OIII}]\lambda\lambda 4959, 5007$ shift	may show blueshift	agrees with $\text{H}\beta_{\text{NC}}$
width FeII	equal to $\text{H}\beta_{\text{BC}}$	may be less than $\text{H}\beta_{\text{BC}}$
optical variability	possible	higher amplitude
X ray variability	can be extreme	possible
Soft X photon index	can be large ($\gtrsim 2 - 4$)	$\lesssim 2$
Radio	predominantly RQ	RQ and RL
BALs	extreme BALs	less extreme BALs
ionization	lower	higher
LIL em. region n_e	higher	lower

3 Inferences on the Broad Line Region Structure

Two observational strategies have been proved to be very powerful to investigate the structure of the broad line region: reverberation mapping [100, 176] and statistical inter-profile comparisons, especially between HILs and LILs [31, 50, 138]. Two dimensional reverberation mapping (i.e., mapping done considering narrow radial velocity intervals in the line profile) requires special observational capabilities, and attempts to perform such measurements have yet to provide convincing results on BLR structure [100]. The correlations of

E1 already allow to organize data in a fashion that provides also appropriate input to reverberation mapping studies. Table 1 summarizes the main trends along the E1 sequence from large $\text{FWHM}(\text{H}\beta_{\text{BC}})$ and low R_{FeII} , to the narrowest $\text{FWHM}(\text{H}\beta_{\text{BC}})$ and largest R_{FeII} .

3.1 A Different BLR Structure Separates Two AGN Populations

An obvious question is whether there is a continuity in properties all across the sequence in the optical E1 plane. This does not seem to be the case. Three results stand out:

1. a discontinuity cannot occur at $\text{FWHM}(\text{H}\beta_{\text{BC}}) \approx 2000 \text{ km s}^{-1}$, the formal limit of NLSy1s, since sources show continuity in properties at least up to $\text{FWHM}(\text{H}\beta_{\text{BC}}) \approx 4000 \text{ km s}^{-1}$ [229]. For example, ultra-soft sources are found at $\text{FWHM}(\text{H}\beta_{\text{BC}}) \approx 3000 \text{ km s}^{-1}$ [27];
2. at $\text{FWHM}(\text{H}\beta_{\text{BC}}) \approx 4000 \text{ km s}^{-1}$ we observe a rather abrupt change in $\text{H}\beta_{\text{BC}}$ profile shape;
3. large $\text{CIV}\lambda 1549$ and $[\text{OIII}]\lambda\lambda 4959, 5007$ blueshifts occur for $\text{FWHM}(\text{H}\beta_{\text{BC}}) \lesssim 4000 \text{ km s}^{-1}$. Fig. 8 shows a correlation between $\text{FWHM}(\text{CIV}\lambda 1549_{\text{BC}})$ and $\text{CIV}\lambda 1549$ peak shift that is valid for RQ Pop. A sources only; the same variables for Pop. B sources would show a scatter plot.

These results have strong structural implications for the BLR. The simplest model able to explain $\text{H}\beta_{\text{BC}}$ and $\text{CIV}\lambda 1549$ properties for sources with $\text{FWHM}(\text{H}\beta_{\text{BC}}) \lesssim 4000 \text{ km s}^{-1}$ is a disk and wind system. An optically thick, geometrically thin disk emits most of $\text{H}\beta_{\text{BC}}$ and all of FeII ; optically thin gas with an outflow radial velocity component v_{out} emits $\text{CIV}\lambda 1549$ and other HILs ([25, 155, 190]; due to the absence of intervening absorption we may expect that the material is highly ionized). The optically thick disk obscuring the receding part of the flow and leaves a net blueshift in the $\text{CIV}\lambda 1549_{\text{BC}}$ line profile [4, 62, 138]. Other lines, like $\text{SiIII}\lambda 1892$ and $\text{CIII}\lambda 1909$ are most probably emitted at the base of the flow in the LIL emitting regions as also suggested by some reverberation mapping results [176]. This model introduces a dependence on the aspect angle θ that can be strongly different for HIL and LILs.

Observations first supported this scheme in the context of a RQ/RL comparison [62, 138]. It seems now that a more meaningful comparison is between sources with $\text{FWHM}(\text{H}\beta_{\text{BC}}) \lesssim 4000 \text{ km s}^{-1}$ (note that this boundary may be somewhat luminosity-dependent, §8.4.1), and the rest of type-1 AGNs [229] because sources with $\text{FWHM}(\text{H}\beta_{\text{BC}}) \gtrsim 4000 \text{ km s}^{-1}$ can be both RL and RQ, and their broad line spectra can be indistinguishable. The evidence in favor of this model is not only statistical but also based on detailed inter-profile comparisons and monitoring of individual sources. For example, NLSy1s IRAS 13224–3809 and 1H 0707–495 are characterized by very blue continua; broad, strongly blueshifted HIL $\text{CIV}\lambda 1549$ and $\text{NV}\lambda 1240$; narrow, symmetric intermediate-ionization lines (including $\text{CIII}\lambda 1909$, $\text{SiIII}\lambda 1892$, and $\text{AlIII}\lambda 1808$) and LILs like $\text{MgII}\lambda 2800$ centered at the rest wavelength [131]. In NGC 4051, the $\text{HeII}\lambda 4686$

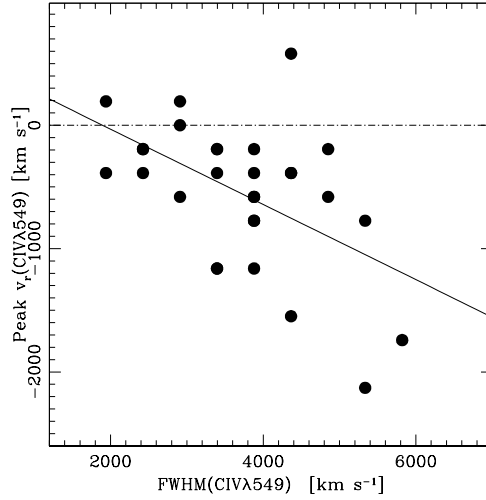


Figure 8: Correlation between $\text{CIV}\lambda 1549_{\text{BC}}$ shift and FWHM for radio quiet, Population A ($\text{FWHM}(\text{H}\beta_{\text{BC}}) \lesssim 4000 \text{ km s}^{-1}$) sources. A formal least-square fit is shown.

line is almost five times broader than $\text{H}\beta$ and is strongly blueward asymmetric. Variability and single-epoch data are consistent with the Balmer lines arising in a low-inclination (nearly face-on) disk-like configuration, and the high-ionization lines arising in an outflowing wind, of which the near side is preferentially observed [180]. Akn 564 is the most extensively monitored NLSy1 galaxy in the UV [40]. Absence of response in the canonical HIL $\text{CIV}\lambda 1549$ line is consistent with matter-bounded emission.

3.1.1 Extreme BAL QSOs as Extreme Pop. A Sources

Assembling the previous results with the main constraint set by much earlier work (see, e. g., Ref. [64]) can lead to a simple geometrical and kinematical model which encompasses Pop. A sources as well as BAL quasars (see Fig. 9). The full blueshift of the emission component of $\text{CIV}\lambda 1549$ (as in Fig. 6) requires that the opening angle of the flow is $\Theta \lesssim 100^\circ$. Closer to the boundaries of the outflow and beyond the BLR proper extends the BAL region in a conical corona of divergence angle $\lesssim 10^\circ$. Whenever a secondary absorption is present (Fig. 6; see also Ref. [117] for an atlas of BAL profiles), we may observe an axial region covering all of the continuum-emitting region and part of the BLR as well [225]. The depth of the absorption implies $f_c \gtrsim 0.5$. It is important to stress that a shell of absorbing material which could provide an adequate f_c is not viable in the geometrical context of our model because of the absorption relatively narrow width. Bent flow lines seen at large viewing angle or along the flow could give rise to NAL and BAL respectively [64]. They would require an opening angle $\sim 180^\circ$, which does not seem supported by the $\text{CIV}\lambda 1549$ profile in our sources. While the cylindrical sheet may appear rather *ad hoc*, it may have a straightforward physical explanation if it is associated to the axial flows which are likely

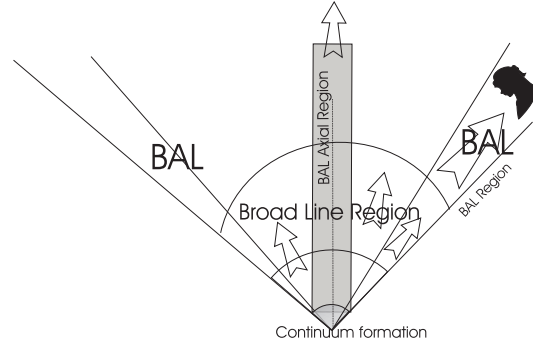


Figure 9: Schematic view of the central engine of extreme Population A sources. The region co-axial with the disk is postulated because of the presence of a secondary, broad absorption in most classical, low- z BAL QSOs. It may be present only in sources with significant black hole spin.

present if the black hole spin is significant (§5).

3.1.2 On the Structure of Population B Sources

The observational structural constraints are by far more ambiguous for Pop. B sources where we do not find a kinematical decoupling between HILs and LILs [62]. This is not to say that a disk and wind system is not applicable, but that the evidence in favor of a wind is less compelling, probably because the ratio between outflow velocity and rotational velocity $v_{\text{out}}/v_{\text{rot}}$ is much lower than in Pop. A sources. It is possible to fit the HIL profiles of Pop. B source NGC 5548 with a wind model, with parameters consistent with reverberation mapping results [39]. Modest outflows ($\sim 1000 \text{ km s}^{-1}$) are seen also in Pop. B sources like NGC 3783 [120]. A mild stratification can explain why higher ionization lines show broader profiles [142]: the FWHM of $\text{HeII}\lambda 4686$, $\text{H}\beta_{\text{BC}}$, and FeII decreases in this order. A “split” BLR explains the same trend in Pop. A [4] and why the $\text{HeII}\lambda 4686$, HeI , and $\text{H}\beta$ lines respond to continuum change with increasing delay in Mkn 110 [114, 111].

3.2 The BLR and the Accretion Disk/Wind Paradigm

Emission lines originating from a geometrically thin, optically thick disk [44] will show extremely small FWHM when observed face-on. Observed properties of CD RL sources suggest that we need a considerable velocity dispersion in the vertical direction to account for observed LIL widths ($\text{FWHM}(\text{H}\beta_{\text{BC}}) \approx 3000 \text{ km s}^{-1}$). A candidate for the line emitting region involves the outer, self-gravitating part of the disk [42, 14]. At some distance r_{SF} the disk is expected to become gravitationally unstable and to dissolve into individual self-gravitating clouds or rings. For the face-on case, assuming orbital motion with Keplerian angular velocity (Ω_K), one can write:

$$\text{FWHM}(\text{H}\beta_{\text{BC}}) \simeq \Delta v \simeq \nu \Omega_{\text{K}} R_{\text{SG}},$$

where Δv is the vertical velocity dispersion, assumed to be proportional to the Keplerian velocity by a factor of ν . A reasonable guess for ν is about 0.1–0.2. One can easily show that FWHM of $\approx 1000 \text{ km s}^{-1}$ implies an $r_{\text{SF}} \sim 5000 R_{\text{g}}$, and 3000 km s^{-1} implies $r_{\text{SF}} \sim 500 R_{\text{g}}$. The Toomre stability criterion applied to a standard Shakura–Sunyaev disk [211] yields results dependent on the assumption of the dominant source of opacity, making the \dot{m} and M_{BH} dependence of r_{SF} highly uncertain [14, 42]. It is however reasonable to conclude that r_{SF} can be smaller in Pop. B sources by a factor ~ 10 , and that this may leave a very “small” emitting surface for any standard optically-thick geometrically-thin disk. Part of the line profile may be produced in the fragmented disk if it is illuminated by a geometrically thick, hot inner region (*Advection Dominated Accretion Flow*, ADAF, or evaporated disk [56]).

The clumpy structure expected for $r \gtrsim r_{\text{SF}}$ may be resolvable through high-resolution spectroscopy. We note also that double-peaked profiles are expected to be resolved if the outer BLR radius is $r_{\text{BLR}} \lesssim 10^5 R_{\text{g}}$. However, double-peaked line profiles from a disk can easily be turned into single-peaked profiles by the presence of a disk wind [155]. Although $v_{\text{out}} \ll v_{\text{rot}}$, the outflow velocity gradient is as large as the rotational velocity gradient. Since photons can escape much more easily along lines of sight with a small projected velocity, the resulting line profiles are single peaked with broad wings even though the emission comes from gas that is essentially on circular orbits [155].

4 Black Hole Mass Determination

4.1 The Virial Assumption

One can estimate the mass of the supermassive black hole using $\text{FWHM}(\text{H}\beta_{\text{BC}})$ and a reverberation BLR “radius” r_{BLR} [108] along with the assumption of virialized motions [123]. The virial mass is

$$M_{\text{bh}} = f \frac{r_{\text{BLR}} v^2}{G},$$

where G is the gravitational constant. If $v = \text{FWHM}$ of a suitable line, $f \approx \sqrt{3}/2$ if the orbits of the BLR gas elements are randomly oriented.

The first question is whether the virial assumption is consistent with the data. If the virial assumption is valid, the BLR dynamics should be dominated by the gravity of a central point mass. In this case the characteristic line broadening should correlate with the time lag for different lines. The virial relationship is only marginally consistent with the best time-delay data [179, 123]. However, emission line profiles of Pop. A sources are relatively symmetric and smooth [140], and the optically thick part respond in a roughly symmetric fashion to continuum changes in 3C 390.3 [217] and NGC 5548 [218]. In the following, we will discuss the appropriateness of the virial assumption to derive M_{BH} considering the

correlations and trends along the E1 sequence of § 2, as well as the structural constraints on the BLR derived in § 3.

4.2 Photoionization Mass

The first estimates of M_{BH} were based on the rough similarity of AGN spectra, and on the consequent assumption of constant ionization parameter U or of constant product Un_e ([262] and references therein). A cumbersome evaluation of the ionizing luminosity is still needed with these methods. Even if these estimates are very rough, and the assumption of constant U is debatable (but see Ref. [150]), these studies provide a consistency check for photoionization models and reverberation mapping results [262]. Further refinements may be possible when the behavior of U along the E1 sequence will be better understood and if FeII can be used to constrain ionizing photon flux and n_e [139, 250].

4.3 Mass Determination through Reverberation Mapping

The distance of the BLR r_{BLR} can be deduced from reverberation data, most notably from $H\beta_{\text{BC}}$ data. The cross correlation function between the continuum and the emission line light curve measures a time lag t_L between continuum and line variations. The time lag, due to the light travel time across the broad line emitting region, yields an estimate of the $r_{\text{BLR}} \approx ct_L$. It is important to stress that the derivation of r_{BLR} follows from several assumptions: (1) the continuum emitting region is much smaller than the line emitting region; (2) observable and H γ ionizing continuum are related. This assumption seems to hold well since the monochromatic luminosity at UV selected wavelengths strongly correlates with r_{BLR} [150, 256]; (3) the light travel time across the BLR is a most important parameter, in the sense that it is shorter than the dynamical time (so that the BLR structure is not changing over the light travel time); (4) no dynamical effects of radiation are considered. Some peculiar structures in the line profiles may however derive from radiation pressure [137]; (5) the line response is linear. The responsivity of the Balmer lines are generally anticorrelated with the incident photon flux. Thus, the responsivity vary with distance within the BLR for a fixed continuum luminosity and changes with time as the continuum source varies [116]. More technical problems involve unevenly sampled data, errors in flux calibration, normalization of spectra (different setup, aperture effects), and dilution by stellar continuum [176, 100]. The coupled effects of a broad radial emissivity distribution, an unknown angular radiation pattern of line emission, and suboptimal sampling in the reverberation experiment can cause systematic errors as large as a factor of 3 or more in either direction [123].

The line FWHM observed at a single epoch is not necessarily the best estimator of the gas velocity dispersion. The highest precision measure of the virial product is obtained by using the cross-correlation function centroid (as opposed to the cross-correlation function peak) for the time delay and the radial velocity dispersion of the variable part of the line [184, 179]. The velocity dispersion for the variable part of the spectrum (which is due to portion of the BLR that is truly optically-thick) has now become available for 35 sources

[179]. With those data Peterson et al. [179] found that the random component in the error of reverberation-based M_{BH} measurements is typically around 30%.

4.3.1 Extending Reverberation Mapping Results through the BLR Size-Luminosity Relationship

It is now common to estimate M_{BH} by assuming that the BLR distance from the central continuum source is $r_{\text{BLR}} \propto (L_{5100})^\alpha$ and $\alpha = 0.6 - 0.7$, as derived from the reverberation data by Kaspi et al. ([108]; §4.3.1). We therefore can write the black hole virial mass as follows: $M_{\text{BH}} \propto \text{FWHM}(\text{H}\beta_{\text{BC}})^2 (\lambda L_{5100})^\alpha$, where L_{5100} is the specific luminosity at 5100 Å in units of $\text{ergs s}^{-1} \text{Å}^{-1}$ [143].

Any deviation from $\alpha = 0.6 \div 0.7$ has quantitative effects. The mass of luminous quasars at $z \gtrsim 0.4$ has been computed by extrapolating this relationship, so that it is important to stress that the relationship is based exclusively on quasars of $z \lesssim 0.4$ and that the high (and low) luminosity ranges of the correlation are poorly sampled. If we consider sources in the luminosity range $43.4 \lesssim \log L/L_\odot \lesssim 45$ (i.e. where the sources in Ref. [108] show uniform luminosity sampling), the slope of the best fit is $\alpha = 0.8$, and could easily be as high as $\alpha = 1$ without increasing significantly the fit standard deviation. This case may be appropriate even for the PG quasar luminosity range [139]. In dwarf active galaxies, $\alpha \approx 0.5$ seems appropriate i.e., dwarf active galaxies show larger BLRs than the values predicted by the $r_{\text{BLR}} - \nu L_\nu$ relation for more luminous AGNs [264]. One must remain open to the possibility that $0.5 \lesssim \alpha \lesssim 1$, and that α might even be a function of L . Changing α implies an L -dependent change in mass estimates: the slope of the luminosity-to-mass relationship is affected as well as the location of points in the $L_{\text{bol}}/M_{\text{BH}}$ vs. M_{BH} diagram in Fig. 13. If a restriction is made to the most likely α range, $\alpha = 0.6 \div 0.7$, the effect on M_{BH} estimates is ≈ 0.2 dex [149].

Summing up all sources of uncertainty, individual M_{BH} obtained from single-epoch $\text{H}\beta_{\text{BC}}$ observations and from the $r_{\text{BLR}} - \text{luminosity}$ correlation seems to be affected by errors as large as a factor 2 – 3 at 1 σ confidence level [256, 179].

4.4 M_{BH} Estimation through an Optically Thin VBLR

Reverberation mapping-based M_{BH} determinations are probably affected by the non-negligible size of the BLR that is optically thick to the Lyman continuum, so that the derived r_{BLR} is not a very well defined quantity. The presence of high-velocity, optically thin line emission is likely rather common in AGNs ([214, 232] and references therein). Typical supporting evidence includes variability in the $\text{H}\beta_{\text{BC}}$ line core, coupled with the absence of variability in the line wings, or strong response in $\text{HeII}\lambda 4686$ without change in $\text{H}\beta_{\text{BC}}$. Observations of quasar PG 1416–129 revealed a large decline in its continuum luminosity over the past 10 years [232]. In response to the continuum change, the “classical” broad component of $\text{H}\beta$ almost completely disappeared (the flux decreased by a factor ≈ 10). A redshifted very broad component $\text{H}\beta_{\text{VBC}}$ persisted after the demise of the broad component [232]. In an optically thick medium the intensity of a recombination line is

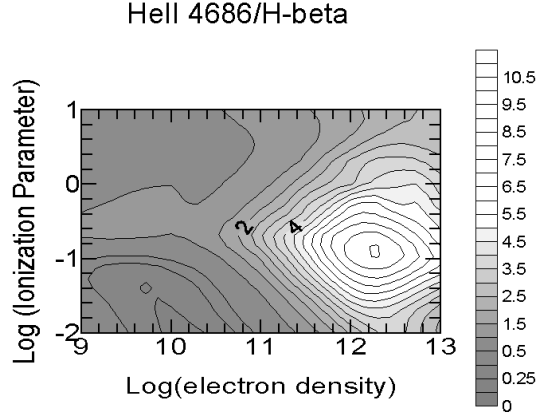


Figure 10: Behavior of the intensity ratio $\text{HeII}\lambda 4686/\text{H}\beta_{\text{BC}}$ as a function of the ionization parameter U and electron density n_e .

governed by the luminosity of the ionizing continuum. If the medium is optically thin the intensity of the same recombination line is governed by the volume and density of the emitting gas and is not directly related to the luminosity of the ionizing continuum. The $\text{H}\beta_{\text{VBC}}$ luminosity can be written as:

$$L(\text{H}\beta_{\text{VBC}}) = 4\pi r_{\text{VBLR}}^2 n_e^2 h\nu_1 \alpha_1 \Delta r,$$

where α_1 and ν_1 are the effective recombination coefficient and the line frequency for $\text{H}\beta$, r_{VBLR} is the distance from the central continuum source of a shell of density n_e and $f_c \approx 1$. The unknown r_{VBLR} can be computed given the luminosity of $\text{H}\beta_{\text{VBC}}$ after having inferred n_e from the *profile* ratio in the line wings of $\text{HeII}\lambda 4686$ and $\text{H}\beta$ ([136, 115]; see Fig. 10 for the expected dependence of the $\text{HeII}\lambda 4686/\text{H}\beta$ intensity ratio). r_{VBLR} is a well-defined quantity because $\Delta r \ll r$ if the optical thickness to the Lyman continuum is less than unity at $n_e \gg 10^{10} \text{ cm}^{-3}$. In principle, if we could be sure that the wings of the Balmer lines are due to optically thin gas, the determination of r_{VBLR} would be possible even from a single line profile observation of $\text{H}\beta_{\text{BC}}$, if the density and the covering factor are known. It is tempting to consider the FWZI and the luminosity of the non-variable part of the line profile of $\text{H}\beta_{\text{BC}}$ from reverberation mapping spectra. This approach could be attempted in the near future since excellent data are now becoming available from reverberation campaigns [179].

4.4.1 Not Only Gravitational Redshift

The amplitude of the redward $\text{H}\beta_{\text{BC}}$ asymmetry observed in Pop. A sources seems to be mass dependent [143]. A factor ≈ 6 increase in the redward displacement of the $\text{H}\beta_{\text{BC}}$ centroid at 1/4 peak intensity [$c(1/4)$] means that the $\text{H}\beta_{\text{BC}}$ asymmetry may be due to gravitational and transverse redshift [49]. A non-Doppler shift is due to a purely gravitational term $\approx GM_{\text{BH}}/r_{\text{BLR}}$. A second term is due to Doppler transverse shift, which is \approx

$1/\gamma$, where γ is the Lorentz factor. If gas motions are virial at $r_{\text{BLR}}(\gg R_g)$, the two terms yield a shift

$$\Delta z \approx \frac{3}{2} \frac{GM}{c^2 r_{\text{BLR}}}.$$

The Pop. B sources considered by a recent study [143] have been subdivided in narrow ranges of M_{BH} and $L_{\text{bol}}/M_{\text{BH}}$. In the range $3.5 \lesssim \log L_{\text{bol}}/M_{\text{BH}} \lesssim 3.9$, the resulting r_{VBLR} values are ≈ 0.005 pc and 0.01 pc for $\log M = 8$ and $\log M = 9$ respectively, if we take the $c(1/4)$ value as a conservative estimate of the redshift. If we also model the VBLR as a gas shell ($f_c \approx 1$) with optical depth to the Lyman continuum $\tau \lesssim 1$, CLOUDY [71] simulations show the shell emission falls far short in explaining the VBLR luminosity [143]. The difference between the expected and observed VBLR luminosity is largely a consequence of the small shell radius required to explain the large Δv_r in the $c(1/4)$. We conclude that, even if $c(1/4)$ is mass dependent, the $c(1/4)$ shift amplitude cannot be explained by gravitational and transverse redshift *alone* [138].

4.5 M_{BH} and Host Mass

It seems that luminous ($-24 > M_V > -28$) quasars (both RL and RQ) are hosted in galaxies which are spheroidal or, at least, possess large bulges [73]. A correlation of nuclear black hole M_{BH} with stellar bulge velocity dispersion σ_* is now well established in nearby galaxies [72, 166]. Supermassive black holes in galactic nuclei are though to be closely related, even in an evolutionary sense, to the bulge of the host galaxy. Reverberation-based M_{BH} estimates can be calibrated using the correlation between M_{BH} and σ_* , even if indirectly (i.e., one cannot use the same objects unless the luminosity drops so much that σ_* becomes measurable; [160]). Seyfert galaxies (if we exclude NLSy1s, [145]) follow the same M_{BH} relation as nonactive galaxies, indicating that reverberation mapping measurements are consistent with those obtained using other methods [166]. Results based on the reverberating part of $\text{H}\beta_{\text{BC}}$ [179] suggest that the systematic uncertainty in the M_{BH} is less than a factor of 3 [166]. The relationship between M_{BH} and σ_* should be taken with care at low M_{BH} . NLSy1s seem to be often host in dwarfish galaxies [119]. Analysis of PG quasar observations suggests a nonlinear relation between M_{BH} and bulge mass ($M_{\text{BH}} \approx M_{\text{bulge}}^{1.53 \pm 0.14}$) although a linear relation cannot be ruled out [126]. The mean $M_{\text{BH}}/M_{\text{bulge}}$ ratio may drop from 0.5% in bright ($M_V \sim -22$) ellipticals to 0.05% in low-luminosity ($M_V \sim -18$) bulges (see also Ref. [145]).

Even more uncertain is the relationship between M_{BH} and bulge absolute magnitude. Seyfert galaxies are offset from nonactive galaxies but the deviation can be entirely understood as a difference in bulge luminosity, and not in M_{BH} ; Seyfert galaxy hosts are brighter than normal galaxies for a given value of their velocity dispersion, perhaps as a result of younger stellar populations [160]. We indeed observe post-starburst quasars i.e., type-1 AGNs that also display the strong Balmer jumps and high-order Balmer absorption lines characteristic of a very massive stellar population with ages ~ 100 Myr, even if they are a few percent of the quasar population [175].

4.5.1 Mass Determination from [OIII] $\lambda\lambda$ 4959,5007

In high-luminosity quasars, the relationship between M_{BH} and σ_* can be studied comparing M_{BH} derived from the width of the broad $\text{H}\beta_{\text{BC}}$ line and M_{BH} from the width of the narrow [OIII] $\lambda\lambda$ 4959,5007 lines used as a proxy to measure σ_* . RQ AGNs seem to conform to the established $M_{\text{BH}}-\sigma_*$ relationship up to values of $M_{\text{BH}} \sim 10^{10} M_{\odot}$, with no discernible change in the relationship out to $z \approx 3$ [220]. There are two major difficulties here. Even if an $M_{\text{BH}} - \text{FWHM}([\text{OIII}]\lambda 5007)$ correlation is present [161], scatter is large. $\text{FWHM}([\text{OIII}]\lambda 5007)$ measures may not always provide a way to estimate M_{BH} . M_{BH} values from [OIII] $\lambda\lambda$ 4959,5007 can be considerably higher than values calculated using $\text{FWHM}(\text{H}\beta_{\text{BC}})$ [143]. This is not surprising because NLSy1-type AGNs apparently do not follow the same relationships as other type-1 AGNs [145]. It is important to stress that low- $W([\text{OIII}]\lambda\lambda 4959,5007)$ sources can have $\text{FWHM}([\text{OIII}]\lambda\lambda 4959,5007) \gtrsim \text{FWHM}(\text{H}\beta)$, invalidating the virial assumption. Blueshifted [OIII] $\lambda\lambda$ 4959,5007 emission arises in outflowing gas possibly associated to a disk wind [288]. The NLR in blue outliers may be very compact and its velocity field is not likely to be dynamically related to the host galaxy stellar bulge. This points to a limiting $W([\text{OIII}]\lambda 5007)$ below which $\text{FWHM}([\text{OIII}]\lambda 5007)$ ceases to be a useful mass estimator. Only large $W([\text{OIII}]\lambda 5007)$ RQ sources in Pop. B may have very extended NLR whose motions is dominated by gravity due to bulge stars.

4.6 Masses of “Special” Sources

4.6.1 “Double Peakers”

A small fraction of AGNs exhibits exceptionally broad, double peaked LILs. The $\text{H}\alpha_{\text{BC}}$ emission line profile is strikingly peculiar (see Ref. [229] for a few typical examples, or recent surveys such as the ones of Refs. [67, 216]). AGNs with double peaked LILs remain relatively rare specimens, even if the SDSS has allowed to identify ~ 100 sources: $\approx 4\%$ (with many dubious cases) of all RQ and RL SDSS sources [216]. Although predominantly RQ, they are more likely to be found in RL sources, and account for about 20% of RL AGNs [216, 67]. Their relative rarity and their exceptionally broad lines prompted workers to search for a specificity either in terms of peculiar views or physics soon after the discovery of the prototypical source Arp 102B [235].

Prototype “double-peakers” Arp 102B, 3C 390.3, and 3C 332 have been now monitored for more than 20 years [132]. A common property of double-peaked lines is slow, systematic variability of the profile shape on a timescale of years i.e., the timescale of dynamical changes in accretion disks [67, 163]. Lower limits on the plausible orbital periods from the absence of peak radial velocity changes would require supermassive binary black holes [82] with total masses in excess of $10^{10} M_{\odot}$. Such large M_{BH} values are difficult to reconcile with a maximum expected limit $M_{\text{BH}} \sim 3 \cdot 10^9 M_{\odot}$ (§4.8; [66]), and with the known $M_{\text{BH}} - \text{host bulge mass}$ relationship. Other recent results from a five year monitoring of $\text{H}\beta$ further support the dismissal of the binary black hole hypothesis for 3C390.3 on the basis of the masses required [217]. Hot spots, spiral waves and elliptical accretion

disks have been recently favored [132, 224]. If the hot spot lies within the accretion disk, it is possible to estimate M_{BH} and also the BLR physical size. The determination of r_{BLR} in physical units removes the degeneracy due to the rotational velocity field (i.e., the velocity scales as $(M_{\text{BH}}/r)^{-0.5}$; disk model profiles yield a distance normalized to R_g). $M_{\text{BH}} \approx (2.2 \pm 0.7) \cdot 10^8 M_{\odot}$ was inferred from the period and the distance of the hot spot in Arp 102B ($4.8 \cdot 10^{-3}$ pc; [163]). It is interesting to note that, within the framework of the model, $M_{\text{BH}}/r \approx 3 \cdot 10^{25} \text{ g cm}^{-1}$ is still below the formal requirement for a black hole but the implied density $\rho \gtrsim 10^{14} M_{\odot} \text{ pc}^{-3}$ is a stringent limit. The M_{BH} in double peakers can be also estimated using the empirical relationship between r_{BLR} and optical continuum luminosity [108]. M_{BH} and \dot{m} computations have been carried out for 135 objects from the SDSS [283] and from a survey of RL broad emission line AGNs [67]. M_{BH} values range from $3 \cdot 10^7 M_{\odot}$ to $5 \cdot 10^9 M_{\odot}$, and \dot{m} is between 0.001 and 0.1. Double peakers are found up to $L \sim 10^{46} \text{ ergs s}^{-1}$.

4.6.2 Black Hole Binaries

Several observational properties of extragalactic radio jets, such as bending, misalignment, and wiggling (often associated with knots superluminally moving along different-scale curved trajectory) have been interpreted in terms of helical structures of the jets. This structure is likely caused by the precession of the jet in a binary black hole system [35, 37, 47, 171, 260]. In the case of OJ 287 the bending of the VLBI jet was reported in Ref. [259]. A very small change in the orientation of the jet is needed in order to change the Doppler boosting dramatically, thereby producing long-term periodic brightness modulations. OJ287 was first recognized as a candidate binary black hole system by noticing the regularly spaced outburst pattern in its historical optical light curve [223]. Photographic information on the brightness of this blazar (thought to be a variable star) extends for about 100 years. Even though the observations were scanty in the beginning, there still was a convincing pattern which led to the prediction of the next major outburst in OJ287 in the fall of 1994. For the first time a predicted cyclic phenomenon was indeed observed in an extragalactic object [222]. Sillanpää et al. [223] modelled the periodic outbursts using a binary system consisting of a pair of supermassive black holes with an orbital period of 8.9 yr (in the rest frame of OJ 287). The light variations in this model are related to tidally induced mass flows from the accretion disks into the black holes [109]. A variant of this model explains and predicts other features of the observed light curve [128]. The variant allows for relativistic precession in the binary black hole system, and associates the major flares with the times at which the secondary black hole crosses the plane of the disk of the primary. The planes of the disks are perpendicular to each other. The monitoring campaign organized to observe OJ 287 in 1994 gave such a detailed light curve that a unique determination of the orbital parameters was possible. The model gave masses of $10^8 M_{\odot}$ and $1.7 \cdot 10^9 M_{\odot}$ for the secondary and primary black hole respectively, and also predicted an eclipse of the secondary black hole disk by the disk of the primary in 1989. The eclipse was indeed observed [246, 194] in the optical but not in the radio, as expected. The observation of the next predicted flares for 2006 or 2007 (the date depends on the model) will allow to

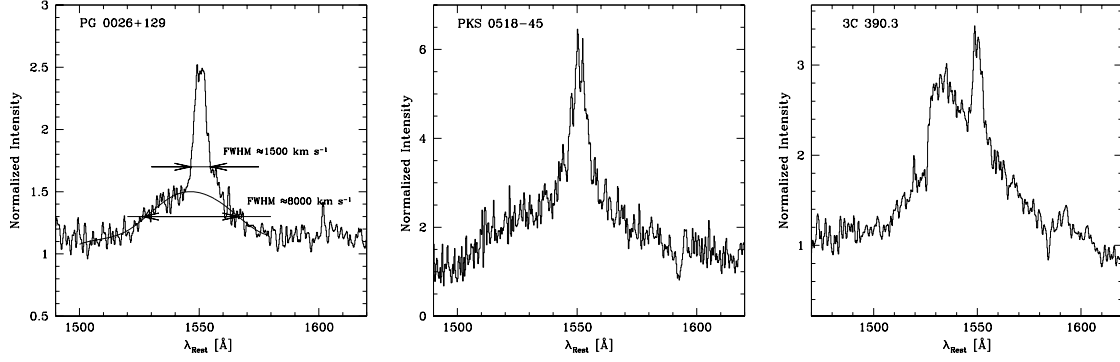


Figure 11: Examples of sources with unambiguous $\text{CIV}\lambda 1549_{\text{NC}}$ emission. The left panel shows two $\text{FWHM}(\text{CIV}\lambda 1549)$ measurements: one for the whole $\text{CIV}\lambda 1549$ profile, and the second one for the $\text{CIV}\lambda 1549_{\text{BC}}$ (thick solid line) only. Neglecting $\text{CIV}\lambda 1549_{\text{NC}}$ results in large $\text{FWHM}(\text{CIV}\lambda 1549)$, and hence M_{BH} measurement errors. The middle and the right panel show two radio loud sources with very high $W([\text{OIII}]\lambda\lambda 4959,5007)$ and widely different $W(\text{CIV}\lambda 1549_{\text{NC}})$.

refine models and make a direct measurement of the orbital energy loss in the system.

4.7 At Low and High z : M_{BH} Determination from $\text{CIV}\lambda 1549$

4.7.1 Existence of a $\text{CIV}\lambda 1549_{\text{NC}}$ Contribution

The very existence of significant $\text{CIV}\lambda 1549$ narrow emission ($\text{CIV}\lambda 1549_{\text{NC}}$) has been a contentious issue. There is plenty of evidence that at least some AGNs with strong narrow lines have a strong $\text{CIV}\lambda 1549_{\text{NC}}$. Perhaps two of the most striking examples are PG 0026+12 (RQ; a borderline NLSy1 with strong NLR emission) and Pictor A (RL; Fig. 11). These are two cases in which an obvious inflection between broad and narrow component is seen, and in which a $\text{CIV}\lambda 1549_{\text{NC}}$ can be easily isolated with $\text{FWHM} \gtrsim 1000 \text{ km s}^{-1}$. The visual impression (already suggested in Ref. [138]) of a connection between $W([\text{OIII}]\lambda\lambda 4959,5007)$ and the $\text{CIV}\lambda 1549$ narrow core is confirmed by a loose correlation between $W([\text{OIII}]\lambda\lambda 4959,5007)$ and $W(\text{CIV}\lambda 1549_{\text{NC}})$ which we found considering *only* the cases of least ambiguous inflection. The data dispersion is probably intrinsic: at the two $\text{CIV}\lambda 1549_{\text{NC}}$ extremes of large $W([\text{OIII}]\lambda\lambda 4959,5007)$ we find Pictor A ($W(\text{CIV}\lambda 1549_{\text{NC}}) \approx 30 \pm 6 \text{ \AA}$) and 3C 390.3 ($W(\text{CIV}\lambda 1549_{\text{NC}}) \approx 5 \pm 1 \text{ \AA}$) with $W([\text{OIII}]\lambda 5007) \sim 80 \text{ \AA}$ (see Fig. 11). We do not expect a strong correlation physically, since emission of $\text{CIV}\lambda 1549$ is favored in the innermost regions of the NLR, as shown below.

Even if RL sources often show prominent $\text{CIV}\lambda 1549$ cores of width $\sim 2000 \text{ km s}^{-1}$, such emission has been ascribed to $\text{CIV}\lambda 1549_{\text{BC}}$ [277] and to an intermediate line region [30]. It is relatively naïve to believe that $W([\text{OIII}]\lambda\lambda 4959,5007)$ and $\text{CIV}\lambda 1549_{\text{NC}}$ should have the same width. Collisionally excited lines such as $\text{CIV}\lambda 1549$ show a band of efficient

reprocessing running at constant U along a diagonal ridge in the plane photon flux versus n_e . Emission is locally optimized along this ridge which corresponds to $\log U \sim -1.5$ for CIV λ 1549 [7]. Provided that a smooth density gradient exists (i.e., that there is a significant amount of gas at $n_e \sim 10^6 \text{ cm}^{-3}$), we expect CIV λ 1549 emission to be strong at larger n_e (CIV λ 1549 emissivity is $\propto n_e^2$ while [OIII] $\lambda\lambda$ 4959,5007 becomes collisionally quenched). If velocity dispersion increases with decreasing distance from the central continuum source it is somewhat natural to expect $\text{FWHM}(\text{CIV}\lambda 1549_{\text{NC}}) > \text{FWHM}([\text{OIII}]\lambda\lambda 4959,5007)$. Detailed calculations based on these simple considerations indeed suggest that $1000 \text{ km s}^{-1} \lesssim \text{FWHM}(\text{CIV}\lambda 1549_{\text{NC}}) \lesssim 2000 \text{ km s}^{-1}$ for a variety of possible density-gradient laws [170, 226]. The same models correctly predict that $\text{FWHM}(\text{H}\beta_{\text{NC}}) \sim 500 \text{ km s}^{-1} \gtrsim \text{FWHM}([\text{OIII}]\lambda\lambda 4959,5007) \ll \text{FWHM}(\text{CIV}\lambda 1549_{\text{NC}})$. To ascribe CIV λ 1549 core emission to the BLR (where $n_e \gtrsim 10^{10} \text{ cm}^{-3}$) seems rather arbitrary. Since CIV λ 1549_{NC} is prominent in Pop. B sources but can be absent in Pop. A., the wind that gives rise to the blue-shifted CIV λ 1549_{BC} component may serve as a filter to the FUV ionizing radiation from the center that would otherwise reach the outer self-gravitating parts of the disk, where CIV λ 1549_{NC} may originate [130].

4.7.2 Is the Width of CIV λ 1549_{BC} a Reliable M_{BH} Estimator?

Estimating M_{BH} from the width of CIV λ 1549 is cumbersome. Failure to account for CIV λ 1549_{NC} has dramatic consequences on M_{BH} and Eddington ratio estimates (§7). Dynamically, the HIL emitting gas is not in virial equilibrium at least in a significant fraction of quasars (§3; Fig. 8). Assuming virial equilibrium for Pop. B (as suggested by the absence of systematic line shifts and by the tentative similarity with the H β_{BC} profile) still leaves the problem of properly assessing CIV λ 1549_{NC}. Recent studies of the CIV λ 1549 profile using HST archival spectra ([12, 122, 121, 256, 266]) have subtracted little or no H β_{NC} from the CIV λ 1549 line profiles. A comparison of line widths and shift measures for H β and CIV λ 1549 [12, 266] shows that there are significant and systematic differences. An apparent dichotomy occurs at $\text{FWHM}(\text{H}\beta_{\text{BC}}) \approx 4000 \text{ km s}^{-1}$ if no CIV λ 1549_{NC} is considered [12]: below 4000 km s^{-1} , the CIV λ 1549 line is broader than H β_{BC} , but the reverse seems to hold when $\text{FWHM}(\text{H}\beta_{\text{BC}}) \gtrsim 4000 \text{ km s}^{-1}$ where we believe that the NLR becomes important (Pop. B; [4]). This result is not necessarily against the view that CIV λ 1549 generally originates closer to the center than H β since CIV λ 1549_{NC} was not subtracted. In the case of PG 0026+129, failure to subtract the NLR emission yields spurious broad line parameter measures (e.g. $\text{FWHM} \sim 8000 \text{ km s}^{-1}$ instead of 1860 km s^{-1} ; see Fig. 11). We conclude that: (a) M_{BH} computations from CIV λ 1549 width are wrong in the case the CIV λ 1549 profile shows large blueshifts i.e., for Pop. A sources; (b) failure to properly correct for CIV λ 1549_{NC} yields a large error in the mass estimate [4]. The M_{BH} error is especially large for Pop. B sources; however, it must be remarked that CIV λ 1549_{NC} can be strong also in Pop. A RQ sources, and that a case-by-case analysis should be made.

4.8 High- z Masses: Are They Really That Big?

If the empirical relationship between r_{BLR} and the source luminosity is used to obtain M_{BH} at high z , the largest M_{BH} are $\gtrsim 10^{10} M_{\odot}$. Such values of M_{BH} suggest bulge mass $\gtrsim 10^{13} M_{\odot}$ and $\sigma_{\star} \gtrsim 700 \text{ km s}^{-1}$ which are not observed at low z . Black holes with $M_{\text{BH}} \gtrsim 3 \cdot 10^9 M_{\odot}$ should reside almost exclusively in high-redshift quasars [169]. This implication is in contrast with the expectation that M_{BH} can only grow with cosmic time on timescales of the Universe present age, and inconsistent with several suggested scenarios of black hole and galaxy formation. A solution of this dilemma may reside in the improper use of CIV λ 1549 as a proxy of H β to estimate M_{BH} . A very good correlation has been recently found between r_{BLR} and the specific continuum luminosity at 3000 Å [150]. In a sample of objects with broad-line radii determined from reverberation mapping the FWHM of MgII λ 2800 and H β are consistent with an exact one-to-one relation, as expected if both H β_{BC} and MgII λ 2800 are predominantly emitted at the same distance from the central ionizing source within a factor of 2.5 [149, 150]. The MgII λ 2800 line seems to be systematically narrower than H β_{BC} probably because MgII λ 2800 (like FeII and the reverberating part of H β_{BC}) is emitted in the most optically thick portion of the BLR. The FWHM(MgII λ 2800) can then be used to estimate M_{BH} of quasars $0.25 \lesssim z \lesssim 2.5$ via optical spectroscopy alone, and it is in principle even preferable to FWHM(H β_{BC}). There are no strong theoretical reasons or empirical evidence to doubt the assumption that the MgII λ 2800 line broadening is virial, at least no more than the ones known for H β_{BC} . FWHM(MgII λ 2800) typically indicates a factor of 5 times lower M_{BH} than CIV λ 1549 [60]. It is interesting to point out that a mass of $3 \cdot 10^9 M_{\odot}$ for the central black hole in the $z = 6.41$ quasar SDSS J114816.64+525150 (one of the most distant quasars known) has been estimated applying the M_{BH} technique appropriate for a detected MgII λ 2800 FWHM of 6000 km s^{-1} [274]. This very high luminosity quasar does not show extremely broad lines and does not require super-Eddington luminosity.

Measurements of H β_{BC} at high $z \gtrsim 1$ can be achieved only through IR spectrometers. Instrumental capabilities lag behind the ones of optical spectrometers, and lack of resolution as well as poor S/N can lead to huge overestimates of FWHM(H β_{BC}) [146], although excellent data for a few tens of sources are becoming available [233].

4.9 Mass Estimates Along the E1 Sequence

The previous results suggest a number of general remarks.

- The most accurate M_{BH} determinations are probably obtained considering the reverberating part of emission lines [179]. If M_{BH} estimates from the reverberating component of H β_{BC} are compared to CIV λ 1549 M_{BH} estimates, offsets of 1.0 dex or larger from a perfect one-to-one relationship are possible [256]. M_{BH} derived from CIV λ 1549 $_{\text{BC}}$ has a probability of just 90% to be within a factor 10 from the best reverberation M_{BH} estimates. For the H β single-epoch estimates, the probability of getting M_{BH} accurate to within an order of magnitude is $\approx 95\%$, which suggests

that systematic sources of uncertainties and ambiguities operate in the estimate of M_{BH} .

- If an innermost region of optically thin (to the Lyman continuum) gas can be identified from the profile of $\text{H}\beta$, an estimate of the line emitting region size is relatively straightforward (§4.4). However, the frequent occurrence of asymmetries partly invalidates the virial assumption for the innermost line emitting regions in Pop. B sources.
- Single epoch, single line M_{BH} determinations based on the FWHM are valid in a statistical sense if the line is a LIL, like $\text{H}\beta$ or $\text{MgII}\lambda 2800$. An estimation of the aspect angle θ is a first-hand necessity, as farther outlined below.
- It is improper to use $\text{CIV}\lambda 1549$ for M_{BH} calculations if the line is blueshifted or strongly asymmetric, as in Pop. A sources. This seems to be the case of most high- z objects [198]. The $\text{MgII}\lambda 2800$ line may provide the best estimator at high z .
- Some special sources, like double peakers and black hole binaries may provide accurate M_{BH} , although r_{BLR} and M_{BH} determinations are still somewhat model dependent. Other sources – like BAL QSOs – may be favored if the orientation angle can be constrained.
- $[\text{OIII}]\lambda\lambda 4959,5007$ may provide a suitable M_{BH} estimator only in RQ sources, predominantly for spectral types A1 and Pop. B, if the recessional velocity from $[\text{OIII}]\lambda\lambda 4959,5007$ agrees with the one deduced from other narrow lines which are of low ionization.

4.9.1 Orientation Effects

As reviewed in the previous sections, there is growing evidence that the LILs are predominantly emitted in a flattened system. LIL emission may be dominated by an extended, optically thick disk in Pop. A, while a fragmented disk may be the main line emitter in Pop. B sources. Inclination relative to a flattened system causes a systematic underestimate of the central mass. This effect is expected to be present in both RQ and RL sources. Considering the vertical velocity dispersion for the line emitting gas at $\theta \rightarrow 0^\circ$ $\text{FWHM}(\theta = 0)$, a suitable parameterization could be $\text{FWHM}(\theta) \approx \text{FWHM}(\theta = 0) + \Delta\text{FWHM} \cdot \sin \theta$, where $\text{FWHM}(\theta = 0) \approx 1000 \text{ km s}^{-1}$ and 3000 km s^{-1} for RQ and RL sources respectively. ΔFWHM can be estimated from the FWHM range from CD to LD sources ([139, 234]; a similar approach has been followed in Ref. [148]). Considering that θ may be in the range $\text{few}^\circ \lesssim \theta \lesssim 45^\circ$, and distributed randomly, we have an average $\langle \theta \rangle \approx 30^\circ$. This means that ignoring orientation effects leads to a systematic underestimate of M_{BH} by $\Delta \log M_{\text{BH}} \approx 0.6$. The underestimate may be a factor $\gtrsim 10$ if the source is observed almost pole-on. Even if pole-on sources are the rarest one in a randomly-oriented sample, errors of this amplitude may dramatically influence inferences on M_{BH} and blur correlations involving $L_{\text{bol}}/M_{\text{BH}}$ (which varies only by 2–3 orders of magnitude in AGNs; §7). It

is also important to consider that optical luminosity may not be appropriate in the $r_{\text{BLR}} - \text{luminosity}$ relationship for CD RL AGNs ($\theta \rightarrow 0^\circ$) because jets may significantly contribute to the optical continuum. A relativistically boosted continuum leads to an overestimation of M_{BH} . In such cases, it may be better to consider an empirical relation between r_{BLR} and the $\text{H}\beta_{\text{BC}}$ luminosity [284].

5 Black Hole Spin & Observer's Orientation

5.1 Where Are Spinning Black Holes?

The idea of a non rotating black hole is rather distressing because every known massive object in the universe (from asteroids to neutron stars) does rotate. Conservation of angular momentum by the accreting matter should lead quickly to maximally rotating black holes [238]. While M_{BH} is destined to increase on timescales comparable to the present age of the Universe, a black hole angular momentum can reverse and decrease through a diversity of mechanisms [80, 101]: the collapse of massive gas accumulations, gas accretion, capture of stellar mass bodies, and successive mergers with other massive holes. A significant black hole specific angular momentum a is required for driving relativistic, radio-emitting jets [17] although a maximally rotating black hole ($a/M \approx 0.998G/c$) is not necessary. In the E1 context, suggestions of $a \neq 0$ come from time scale variability arguments, especially from soft-X ray observations of NLSy1 sources. A variation in luminosity cannot occur on an arbitrarily short time scale, a minimum physical limit being set by the light crossing time of the emitting region. The emitting matter should have some opacity $\tau \approx n\sigma r \sim 1$, where σ is the Thomson scattering cross-section. The time needed for radiation to diffuse out of a region of size r is therefore $\Delta t \approx (1 + \tau)r/c$ [69]. The change in luminosity ΔL following an accretion event with accretion rate $\Delta M/\Delta t$ is $\Delta L = \eta\Delta M/\Delta t c^2$. Writing $\Delta M = \frac{4}{3}\pi R^3 n m_p$ where $n = \tau/\sigma R$ and m_p is the proton mass, and considering the travel time, we have:

$$\frac{\Delta L}{\Delta t} \lesssim \frac{4}{3}\pi \frac{m_p}{\sigma} c^4 \eta \approx 2 \cdot 10^{41} \eta_{0.1} \text{ergs s}^{-1}.$$

If changes of very large amplitude occur in such a short timescale that the relation above is violated for $\eta \approx 0.1$, claims have been laid that a rotating black hole is needed. This has been the case for a handful of NLSy1 galaxies [74]. In the view that some NLSy1s and at least some other Pop. A sources are young/rejuvenated quasars [144, 229, 88], they may have experienced one of few accretion events leading to a consistent increase of the black hole angular momentum.

Two-fluid models for relativistic outflows include a fast, relativistic beam surrounded by a slower, possibly thermal, outflow, with a mixing layer forming between the beam and the jet (e.g., [134]). The mixing layer could produce the secondary absorption seen in several BAL sources (Fig. 6). It is interesting to stress that the observed R_{FeII} for the BAL QSOs Mkn 231 and IRAS 07598+6508 would require highly super-Eddington accretion unless the accreting object is a rotating black hole. Another aspect favoring a maximally

rotating black hole is the remarkable behavior of the Fe $K\alpha$ emission line in MCG –06–30–15 [227]. This source is pretty unremarkable optically; it is a Pop. A source with modest FeII_{opt} emission. More circumstantial evidence favoring rotating black holes is provided by the mass density of supermassive black holes in the present-day universe, which agrees with the quasar luminosity evolution and total power output if the efficiency has been $\eta \gtrsim 0.1$, larger than that of a non-rotating black hole [94].

It is then intriguing that, at present, neither black hole spin nor morphology seem to be sufficient conditions to explain radio loudness [63], disfavoring the idea that the RL and RQ dichotomy may be due to systematically different black hole spins [280]. The physics of radio emission in the inner regions of all quasars (RL and RQ) may be essentially the same, involving a compact, partially opaque core together with a beamed jet [10]. Other factors may be at play: a strong electromagnetic field, coupled with differential rotation, could serve to convert rotational energy into kinetic energy of outflows [34]. In the context of optical/UV observations such effects are at present observationally unconfirmed, also because radio loudness does not seem to have appreciable effects on the observed broad line spectrum [143]. In principle, we could expect that, if a viscous accretion disk is inclined in relation to the equatorial plane of a rotating black hole, the differential precession will produce warps in the disk. The combined action of the Lense-Thirring effect and the internal viscosity of the accretion disk forces the alignment between the angular momenta of the rotating black hole and the accretion disk at $r \sim 1000 R_g \sim r_{\text{BLR}}$. Some double peaked emission line profiles may be produced by warped disks. The agreement between some peculiar H α_{BC} profiles and a toy model is very good [33, 3], but many other models may also be applicable without invoking a warped disk [224].

5.2 Can we Measure an Orientation Angle?

In radio-loud quasars, where a rough orientation indicator is available from the radio core-to-lobe ratio, there is good evidence that FWHM(H β_{BC}) shows an orientation dependence consistent with a flattened (or even disk-like) geometry [275, 29]. There is a domain space separation between Fanaroff-Riley II (i.e., LD) and CD sources in E1. The diagonal arrow in figure 7 indicates the average change in E1 position due to change in orientation from LD to CD sources. As stressed earlier, M_{BH} can be underestimated if no correction is applied to observed LIL widths [167]. An analysis of the connection between M_{BH} and radio luminosity in radio-selected flat-spectrum quasars shows that values of M_{BH} are not systematically lower than those of luminous optically selected RL quasars, if a proper correction for the effects of inclination is applied [105]. It is also unlikely that there are sources radiating at $L_{\text{bol}}/L_{\text{Edd}} > 1$ at $z \lesssim 0.8$ (see Fig. 14; [143]) if a reasonable orientation correction is applied to line widths. While a correction for the effect of varying θ is feasible in a statistical sense, measuring θ on a source-by-source basis has proved to be very difficult. Superluminal radio sources are an exception. Radio observations allow an estimate of the expected synchrotron self Compton flux relative to the observed X-ray flux. Lorentz factor and θ can then be independently estimated [84]. Figure 12 shows θ vs. FWHM(H β_{BC}) for 11 superluminal sources, confirming a factor ≈ 3 effect on the H β_{BC} width at extreme θ

values.

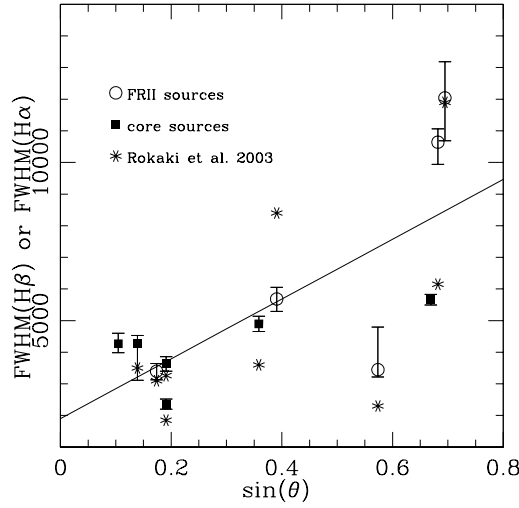


Figure 12: Dependence of $\text{FWHM}(H\beta_{BC})$ on orientation angle θ for superluminal sources [234] with data from Refs. [204, 143].

The observational properties of some, extreme NLSy1s may well be due to a pole-on orientation angle. A NLSy1 nucleus has been found in the extensively studied eruptive BL Lac, 0846+51W1, out of a large sample of NLSy1 from the SDSS [292]. The SDSS allowed the identification of another source with typical NLSy1 properties (strong FeII_{opt} , undetectable $[\text{OIII}]\lambda\lambda 4959, 5007$) that is definitely RL ($R_K \gtrsim 1000$). The inverted radio spectrum and the very high brightness temperature derived from variation of the radio flux suggested the presence of a relativistic jet beaming toward the observer [291]. It is unclear whether this finding can be extended to (at least) some RQ NLSy1s. Some NLSy1 might be considered the radio quiet equivalent of BL Lacs if they give rise to radio-silent relativistic outflow. Even if evidence is accumulating about the existence of a relativistic jet in RQ sources (e.g., [10]), RQ sources (especially if of Pop. A) are not optically violently variable. Although some NLSy1 sources (those with largest $[\text{OIII}]\lambda\lambda 4959, 5007$ and $\text{CIV}\lambda 1549_{BC}$ blueshifts, as well as narrowest $H\beta_{BC}$ and most strongly variable soft X-ray excess) are likely to be oriented almost pole-on, it is still not clear whether we are observing a beaming effect.

Orientation estimates for RQ sources may come from the correlation between Γ_{soft} and soft-X ray variability amplitude, although the poor understanding of the soft X-ray excess prevents the definition of an orientation indicator. Other attempts at estimating θ are rather model-dependent. A sample of several thousand quasars from the SDSS confirms that HILs such as $\text{CIV}\lambda 1549$ are significantly blueshifted with respect to LILs such as $\text{MgII}\lambda 2800$ [198]. Among the SDSS sources, $\text{CIV}\lambda 1549$ emission-line peaks have a range of shifts from a redshift of 500 km s^{-1} to blueshifts well in excess of 2000 km s^{-1} compared to

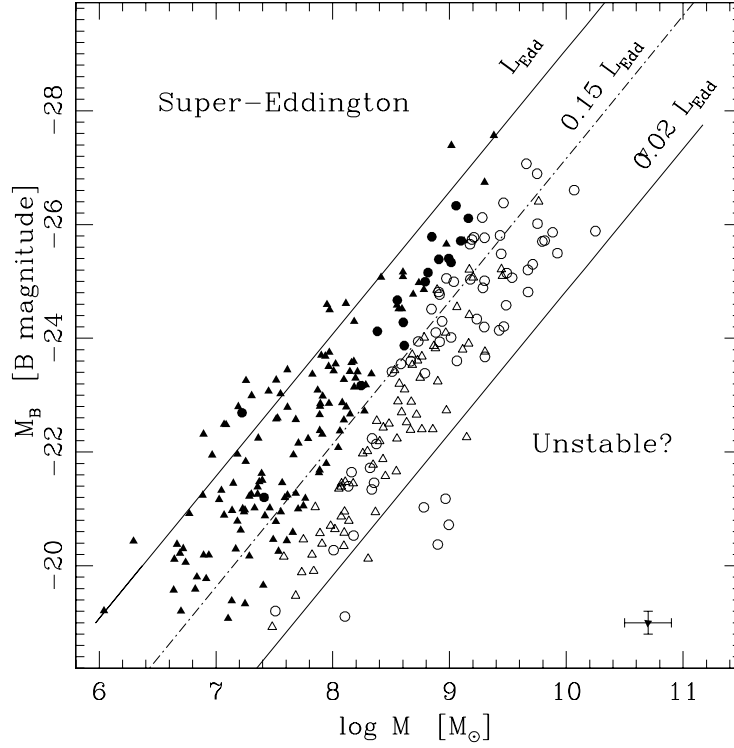


Figure 13: Mass Luminosity relationship for a sample of ≈ 270 AGNs [143]. Triangles and circles indicate radio-quiet and radio-loud sources, respectively. Open symbols indicate sources with $\text{FWHM}(\text{H}\beta_{\text{BC}}) \gtrsim 4000 \text{ km s}^{-1}$ (Pop. B); filled symbols sources with $\text{FWHM}(\text{H}\beta_{\text{BC}}) \lesssim 4000 \text{ km s}^{-1}$ (Pop. A). The bars in the lower right corner indicate typical errors.

$\text{MgII}\lambda 2800$. The anticorrelation between the shift of the $\text{CIV}\lambda 1549$ emission-line peak and $W(\text{CIV}\lambda 1549)$ (Fig. 8) is confirmed by the SDSS study. Composite quasar spectra as a function of $\text{CIV}\lambda 1549$ shift suggest that the apparent shift of the $\text{CIV}\lambda 1549$ emission-line peak is not a shift so much as it is a lack of flux in the red wing for the composite with the largest apparent shift [198]. An outflowing wind and an optically thick disk to act as a screen provide a tempting explanation. However, it is unlikely that purely geometrical effects are at play in determining the width and shifts of $\text{H}\beta_{\text{BC}}$ and $\text{CIV}\lambda 1549_{\text{BC}}$ alike [139], even if a simple toy model shows that $\text{CIV}\lambda 1549$ shift amplitude is orientation dependent with the largest shifts being produced by $\theta \rightarrow 0^\circ$ [288]. $W(\text{CIV}\lambda 1549)$ is strongly dependent on $L_{\text{bol}}/M_{\text{BH}}$ ([4, 12]; see §8.4.1), as are the properties of outflowing winds [155, 190]. To estimate θ on a source by source basis, we first need to understand how $W(\text{CIV}\lambda 1549)$ and $\text{CIV}\lambda 1549$ shifts are affected by $L_{\text{bol}}/L_{\text{Edd}}$ and θ .

We mention here an interesting attempt that is, again, strongly dependent on specific assumptions. Using the variable fraction of the $H\beta_{BC}$, HeI, and HeII λ 4686 profiles to estimate r_{BLR} , and then comparing the virial M_{BH} and the M_{BH} obtained assuming that the variable-fraction shifts observed in Mkn 110 are due to gravitational redshift, a measurement of the spin axis of the central black hole is possible [112]: $\theta \approx 21 \pm 5^\circ$. Unfortunately, there is as yet no convincing general evidence that the redward asymmetry seen in $H\beta_{BC}$ profiles is entirely due to gravitational redshift (§4.4.1).

6 The Mass - Luminosity Diagram

Fig.13 shows a plot of M_B vs. M_{BH} for a combined sample of ≈ 280 AGNs which cover an absolute B magnitude range $-20 \gtrsim M_B \gtrsim -27$ and an M_{BH} interval $10^6 \lesssim M_{BH} \lesssim 10^{10}$ ([143]; cf. Refs. [281, 41]). The wide majority of sources are located between $0.02 \lesssim L/L_{Edd} \lesssim 1.00$. RQ sources show evidence for significant Malmquist bias while RL sources show the opposite trend probably related to a bias towards selecting higher luminosity core-dominated sources likely to be beamed. We find that the Eddington limit defines an approximate upper boundary to the luminosity distribution [281], indicating that there are no low- z AGNs radiating significantly above the Eddington limit (this depends somewhat on the adopted H_0 value). Figure 13 also suggests that there may be fewer high (than low) mass sources with L_{bol}/M_{BH} close to the Eddington limit. This might be a selection effect or an indication that galaxies with large M_{BH} may be unable to supply fuel at high L_{bol}/M_{BH} i.e., a limit on M [165]. If a sample comprising more high luminosity objects ($L \gtrsim 10^{47}$ ergs s^{-1}) is considered, 41% of the objects in that sample with $L \gtrsim 10^{47}$ ergs s^{-1} have super-Eddington ratios [266]. We caution however that correction for orientation and beaming should decrease L_{bol}/L_{Edd} . The lower envelope of the luminosity distribution of Fig. 13 may be due to a selection effect [281], or it may indicate that only sources radiating at $0.01 \lesssim (L_{bol}/L_{Edd}) \lesssim 1.00$ exhibit a stable BLR. The lower limit may be connected with the absence or small size of a standard accretion disk (§7.1; see also Refs. [113, 165]). Redshift evolution of the black hole mass-luminosity ratio is found to be much less than the $(1+z)^3$ evolution seen in QSO luminosity function evolution [48]. This means that quasars radiate in almost the same L_{bol}/M_{BH} range also at high- z .

7 The Eddington Ratio as the Driver of the E1 Correlations

A PCA reveals a first principal component accounting for 48% of the spectrum-to-spectrum variance with just UV emission line strengths, ratios and widths as input. This linear combination of the input variables depends on L_{bol}/L_{Edd} [213, 279]. A reanalysis of PG quasars confirms that E1 is driven predominantly by L_{bol}/L_{Edd} while a second principal component is driven by accretion rate [21]. An UV based spectral PCA that uses the whole spectrum in the rest wavelength interval 1170–2100 Å find consistent results although the relative

importance of luminosity and $L_{\text{bol}}/L_{\text{Edd}}$ is reversed i.e., $L_{\text{bol}}/L_{\text{Edd}}$ appears in a second eigenvector accounting for 20% of the spectrum-to-spectrum variance [285]. The E1 optical sequence and the $L_{\text{bol}}/L_{\text{Edd}}$ trends have been recently confirmed also for intermediate z quasars [162, 233, 287]. Comparison between high and low- z QSOs confirms that the inverse $\text{FeII}_{\text{opt}} - [\text{OIII}]\lambda\lambda 4959,5007$ relationship (i.e., E1) is indeed related to $L_{\text{bol}}/L_{\text{Edd}}$ rather than M_{BH} [287].

Different $L_{\text{bol}}/M_{\text{BH}}$ values explain the change in FeII and $\text{W}(\text{H}\beta_{\text{BC}})$ prominence in the optical plane [139, 278, 162]. The virial relationship can be rewritten in the form of $\text{FWHM}(\text{H}\beta_{\text{BC}}) \propto (L_{\text{bol}}/M_{\text{BH}})^{-1} M_{\text{BH}}^{-0.4}$ using the $r_{\text{BLR}} - \nu L\nu$ correlation. The diagnostic ratios $\text{SiIII}\lambda 1892 / \text{CIII}\lambda 1909$ and $\text{AlIII}\lambda 1808 / \text{CIII}\lambda 1909$ provide an estimate of n_e . Since n_e correlates with $\text{FWHM}(\text{H}\beta_{\text{BC}})$ [278, 139] it is possible to write also the ionization parameter (and R_{FeII}) as a function of $L_{\text{bol}}/M_{\text{BH}}$ and M_{BH} [289]. The E1 “elbow” sequence in the optical plane is reproduced by varying $L_{\text{bol}}/L_{\text{Edd}}$, with $L_{\text{bol}}/L_{\text{Edd}} \rightarrow 1$ toward spectral type A3. Orientation can be modelled as a third parameter in this scheme from the location of CD and LD RL QSOs [234]. Model computations suggest that sources of spectral type A1 are actually almost face-on, low $L_{\text{bol}}/L_{\text{Edd}}$ sources [139]. This result explains why some extremely low $\text{W}(\text{H}\beta_{\text{BC}})$ objects (the second extreme type mentioned in §1.2) are observed in bin A1. Sources of bin B1, A2, A3 are instead rather homogenous in terms of $L_{\text{bol}}/L_{\text{Edd}}$ with M_{BH} and θ acting as source od scatter. It has also been possible to show that the $\text{H}\beta_{\text{BC}}$ different profile shapes of Pop. A and B sources are linked to differences in $L_{\text{bol}}/L_{\text{Edd}}$ [143].

The soft X-ray spectral index correlates extremely closely with Eddington ratio and $\text{FWHM}(\text{H}\beta_{\text{BC}})$ [88, 229, 279]. $\text{W}(\text{CIV}\lambda 1549)$ decreases toward extreme population A (see a more detailed discussion in §8.4, and Fig. 16, where a dependence of $\text{W}(\text{CIV}\lambda 1549)$ on spectral type is clearly shown). Also, the distributions of large $\text{CIV}\lambda 1549_{\text{BC}}$ blueshifts and blue outliers seem to be governed by $L_{\text{bol}}/L_{\text{Edd}}$ ([143, 11, 288]; Fig. 14). Among type 1 AGNs with large blueshifted $[\text{OIII}]\lambda 5007$, there is no correlation between the Eddington ratio and the amount of $[\text{OIII}]\lambda 5007$ blueshifts. However, the Eddington ratios of the blue outliers are the highest among AGNs with the same M_{BH} in a sample of 300 objects [143]. These facts suggest that high $L_{\text{bol}}/L_{\text{Edd}}$ is a necessary condition for $[\text{OIII}]\lambda\lambda 4959,5007$ large blueshifts.

Both NLSy1s galaxies and BAL QSOs of the PG sample lie at the high $L_{\text{bol}}/M_{\text{BH}}$ extreme [21, 139, 287], although these two object classes are well separated in a second eigenvector based on \dot{M} [21]. Other measurements confirm this scenario. BAL quasars show large $\text{CIV}\lambda 1549$ emission blueshifts [197, 225]. Using the luminosity and $\text{H}\beta_{\text{BC}}$ to derive M_{BH} and \dot{m} , both BAL and non-BAL QSOs at $z \sim 2$ tend to have even higher $L_{\text{bol}}/L_{\text{Edd}}$ than those at low z [287]. Extreme Pop. A sources may represent the most intense accretors with extreme BAL QSOs being observed at the largest inclination angles possible for a given wind geometry. A large mass flow may limit the viewing angle range of extreme Pop. A sources to be $\approx 90^\circ$ (§ 3.1.1 & Fig. 9). It is important to stress a possible difference between the most extreme BALs (i.e., those with the highest terminal radial velocity, $\sim 30000 \text{ km s}^{-1}$) and the generality of BAL sources. While the most extreme

BAL QSOs seem to be associated to highest $L_{\text{bol}}/L_{\text{Edd}}$, the presence of a shallow BAL of moderate terminal velocity is not necessarily a signature of high $L_{\text{bol}}/L_{\text{Edd}}$ since the terminal velocity correlates with $L_{\text{bol}}/L_{\text{Edd}}$ if the wind giving rise to the BALs is radiation driven [225, 196, 197].

The separation between Pop. A and Pop. B sources, which may occur at $L_{\text{bol}}/L_{\text{Edd}} \approx 0.15$ (Fig. 13) could be in part explained by a change in accretion mode. We note that there is no correlation between radio loudness R_K and $L_{\text{bol}}/L_{\text{Edd}}$ in a RL sample [92] although RL sources are differentiated in terms of $L_{\text{bol}}/M_{\text{BH}}$ from RQ sources [143]. Most or all of the weakly AGNs in nearby galaxies are RL, highly sub-Eddington systems that are plausibly experiencing advection-dominated accretion [99]. The vast majority of these objects appear to be radiating between 0.01 and 0.1 Eddington luminosity, and may therefore be akin to Pop. B powerful quasars. Radiatively inefficient accretion at less than a few per cent of the Eddington rate is unlikely to produce excess soft X ray emission [152, 159]. Lower mass loss rate, and the harder spectrum (which may decrease radiative acceleration) may both contribute to the absence of a strong wind in Pop. B sources.

7.1 Are “Double Peakers” a Peculiar Population?

Recent work seems to confirm the accretion disk origin of the LILs for double-peakers. Inter-profile comparison between Balmer lines and $\text{CIV}\lambda 1549$ (which, in a few cases, show a markedly different, single peaked Gaussian profile [68]) can be interpreted in the framework of the disk and wind paradigm. More $\text{CIV}\lambda 1549$ – Balmer line profile intercomparisons are needed to reach a firm conclusion also because the $\text{CIV}\lambda 1549$ profiles thus far observed cannot be immediately ascribed to a wind. The LIL emitting portion of the disk to produce double-peaks as separated as in Arp 102B is relatively modest, from $\sim 100 R_g$ to $\sim 500 R_g$ [38]. At smaller radii, a hot solution may be appropriate [159], while at $\gtrsim 500 R_g$ self gravity may dominate. Using the customary empirical relation between the broad-line region size and optical continuum luminosity, M_{BH} and accretion rate have been computed for 135 AGNs with double-peaked broad emission lines from the SDSS from a survey of RL AGNs [283]. The inferred range of M_{BH} of double-peakers cover almost the full range of M_{BH} of type-1 AGNs, $3 \cdot 10^7 M_\odot$ to $5 \cdot 10^9 M_\odot$ and L_{bol} up to 10^{46} ergs s^{-1} [283]. Typical Eddington ratios are 0.001, much lower than the typical type-1 AGN; about 90% of them show $L_{\text{bol}}/L_{\text{Edd}} \lesssim 0.02$ (from the distribution of $L_{\text{bol}}/L_{\text{Edd}}$ shown by [283]). Double-peaked sources lie close to the lower $L_{\text{bol}}/M_{\text{BH}}$ boundary or below in the mass-luminosity diagram.

The evidence reported does not suggest that double peakers are truly peculiar sources, i.e., an independent Population C even if they lie out of the mass-luminosity sequence of Fig. 13. A two-component model assuming that the line wings originate in an accretion disk with additional contribution from spherical emission region fits very well the observed $H\beta_{\text{BC}}$ profiles of Pop. B sources [187, 216]. An evolutionary scheme from single peaked Pop. B and double peakers is at least conceivable: double peakers show, on average, the lowest $L_{\text{bol}}/L_{\text{Edd}}$ (and probably also the lowest \dot{M}). They may be AGNs exhausting their fuel supply, with little gas reservoir, in which only the innermost part of the accretion disk

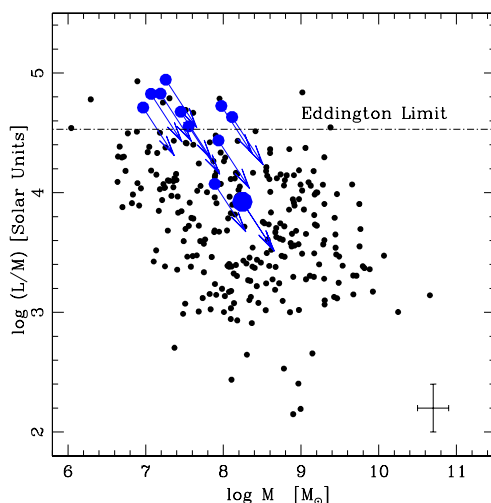


Figure 14: Position of blue outliers (large blue spots) relative to other sources in our sample (filled circles). The largest circle indicates the position of PKS 0736+01, the only known RL blue outlier. The dashed line indicates the Eddington limit. Arrows indicate displacements of blue outliers if we apply an orientation correction 0.4 to the derived masses [140].

is left to produce broad emission lines.

“Naked” AGNs Indirect arguments suggest that some “true” type 2 AGNs do exist [127, 165]. They are AGNs without a hidden BLR even in spectropolarimetric data [240]. The observed radius-luminosity relation for the BLR implies an increasing line width with decreasing luminosity for a given black M_{BH} . However, the upper limit to the observed width of broad emission lines in AGNs at $\sim 25000 \text{ km s}^{-1}$ [229] may reflect a physical limit above which the BLR may not be able to survive [127]. The disappearance of the BLR has been linked to the critical radius at which the disk changes from gas pressure dominated to radiation pressure dominated, or to disk evaporation [56, 164]. For low enough accretion rates, the critical radius becomes smaller than the innermost stable orbit of the accretion disk and the BLR may not form [165]. The intrinsic (i.e., unabsorbed) X-ray luminosity and an estimation of M_{BH} using the relationship between nuclear mass and bulge luminosity in galaxies indicate that all hidden BLR sources have accretion rates $\dot{m} \gtrsim 10^{-3}$. This is also approximately the limit at which double-peakers are found [283]. Naked AGNs may this be observed if $\dot{m} \ll 10^{-3}$.

7.2 On the Origin of Radio Loudness

RL activity in low M_{BH} sources is observed, and there are RL NLSy1s that radiate all $\log L/M \approx 4.5$ [143]. There are no appreciable effects (within the limits set by S/N) on

the $H\beta_{BC}$ profile attributable to radio loudness. Pop. B RL and RQ sources can have the same M_{BH} and L_{bol}/M_{BH} values. Therefore, *it is not unreasonable to conclude that a similar range of M_{BH} and L_{bol}/M_{BH} is physically possible for both RQ and RL sources* [282]. However, this does not mean that the mass function and the L_{bol}/M_{BH} distribution are necessarily the same for RL and RQ sources. RL and RQ sources are well separated in terms of M_{BH} in the E1 space [21] at low z . A robust inference from a bootstrap analysis is that the mass function and the conditional probability of having certain L_{bol}/M_{BH} values at fixed M_{BH} are different for the two AGN classes [143]. With the customary M_{BH} computation assumptions, M_{BH} in RL sources have been found to be $M_{BH} \gtrsim 10^8 M_{\odot}$, while only a few quasars may contain smaller black holes [92]. These conclusions are in agreement with studies based on the SDSS carried out using a sample of more than 6000 AGNs [151]. RL sources were found to harbor systematically more massive black holes than are the RQ quasars with very high significance (see also Ref. [63]). It is important that RQ and RL samples have indistinguishable distributions on the redshift-optical luminosity plane, excluding the possibility that either parameter is responsible for the observed M_{BH} difference [143, 150]. Quasars from the FIRST Bright Quasar Survey [13] fill in the gap between the RL and RQ quasars in the radio vs. optical luminosity plane, show a continuous variation of radio luminosity with M_{BH} and no evidence for a discontinuity that may signal the turning on of powerful radio jets [124]. We suggest that several factors drive the RQ/RL separation in the E1 space: intrinsic mass function and L_{bol}/M_{BH} distribution differences, jet-related effects yielding $[OIII]\lambda\lambda 4959, 5007$ enhancement in RL sources, and sample selection criteria [125, 21, 143]. The range in radio luminosity at a given M_{BH} is several orders of magnitude. Additional parameters other than M_{BH} and L_{bol}/M_{BH} like evolution should be invoked to explain the quasar radio-loudness dichotomy [151].

8 At the Origin and at the End

8.1 Is the Emission Line Width Increasing with Luminosity?

A trend between $FWHM(H\beta_{BC})$ and luminosity is expected if the usual virial and $r_{BLR} - \nu L_{\nu}$ reasonings are applied. There is a well-defined lower boundary in the diagram M_{BH} vs. M_B (see Fig. 15; [233]). Here we make the assumption that low-redshift NLSy1 with the narrowest lines radiate very close to the Eddington ratio. If we assume $\log L_{bol}/M_{BH} \approx 4.5$, we obtain $FWHM(H\beta_{BC})_{min} \approx 600 \text{ km s}^{-1}$ for $\log L = 11$ in solar units and $FWHM_{min}(H\beta_{BC}) \propto 10^{(-0.08M_B)}$. If we consider the luminosity dependence of $FWHM(H\beta_{BC})_{min}$, we see that the expected trend for $\alpha = 0.6$ reproduces fairly well the $FWHM(H\beta_{BC})$ lower boundary as a function of M_B . A less pronounced trend, especially at high luminosity, is expected for $\alpha = 0.7$. The presence of a correlation between $FWHM(H\beta_{BC})$ and luminosity in a survey may depend on sample and intrinsic dispersion of $FWHM$ values in a narrow M_B range. One should consider that *the expected luminosity dependence is very weak*: $\Delta FWHM(H\beta_{BC})$ increases by $\approx 1000 \text{ km s}^{-1}$ over an increase of $\Delta M_B \approx 10$, with $FWHM(H\beta_{BC})_{min}$ changing from 1000 km s^{-1} to 2000 km s^{-1} . In a

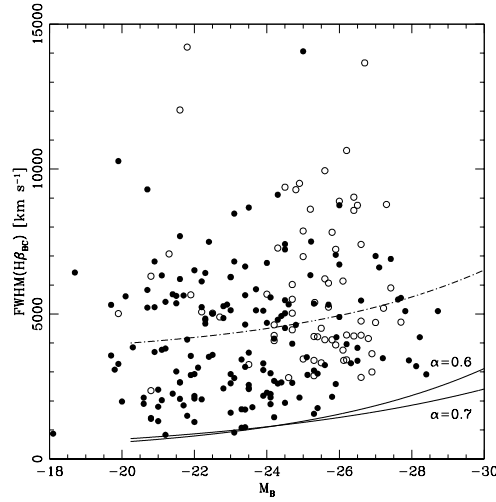


Figure 15: $\text{FWHM}(\text{H}\beta_{\text{BC}})$ in km s^{-1} vs. absolute magnitude M_B for two joined samples, one at low redshift ($z \lesssim 0.8$, [140]), and the other for intermediate redshift quasars [234]. Filled and open circles indicate RQ and RL sources respectively. The dependence on luminosity for the minimum $\text{FWHM}(\text{H}\beta_{\text{BC}})$ and for the boundary between Pop. A and B sources is shown. See text for details.

narrow M_B range, the $\text{FWHM}(\text{H}\beta_{\text{BC}})$ intrinsic scatter spans the range 1000–10000 km s^{-1} , therefore making any correlation intrinsically very weak even if statistically significant. A very large sample from the 2dF and 6dF redshift surveys shows a weak increase of $\text{H}\beta$ line width with luminosity with a slope $\approx 0.15\text{--}0.2$ (Δv vs. $\log L$), very close to the one derived from our calculation [48].

8.2 Lack of Evolution in the FeII Spectrum?

An analysis of the spectra of 12 high-redshift quasars in the region of $\text{MgII}\lambda 2800$ shows remarkable similarity with the LBQS composite ($z \lesssim 0.8$; [237]). Near-infrared spectra of four QSOs located at $z > 6$ have been recently analyzed [103]. Two out of four $z > 6$ QSOs have significant FeII_{UV} . Spectra of three additional sources indicate $\text{FeII}_{\text{UV}}/\text{MgII}\lambda 2800$ similar to that observed in low- z quasars [78, 9]. The $\text{FeII}_{\text{UV}}/\text{MgII}\lambda 2800$ ratio at high redshift should be a factor of 3 lower than for low-redshift QSOs if the age of the universe at the earlier epoch is much less than 1 Gyr [96]. This prediction is due to the delayed contribution of type Ia supernovæ to the iron abundance. Apart from the intriguing results for the highest z quasars, systematic examinations of the $\text{FeII}_{\text{UV}}/\text{MgII}\lambda 2800$ intensity ratio with redshift suggest that the ratio may indeed decline at $z \gtrsim 1.5$ [104, 103]. LBQS spectra show a significant Baldwin effect in FeII_{UV} emission. Further analysis reveals that the primary correlation of iron emission strength is probably with z , implying an evolutionary effect [87]. A very recent SDSS study based on ~ 16000 spectra in the redshift range from

0.08 to 5.41 shows that the dominant redshift effect is a result of the evolution of the blended FeII emission (optical) and the Balmer continuum [285]. This redshift dependence can be explained by the evolution of chemical abundance in the quasar environment, or by an intrinsic change in the continuum itself [285]. In another study [251] quasars were grouped on the basis of their $\text{FeII}_{\text{UV}}/\text{MgII}\lambda 2800$ intensity ratios. The fraction of quasars in each group with strong $\text{FeII}_{\text{UV}}/\text{MgII}\lambda 2800$ dropped significantly at $z \gtrsim 1.5$. To check whether there is a change in iron abundance at high redshifts observations covering FeII_{opt} are essential.

8.3 A Scheme of Physical Evolution for the AGNs

High- z quasars must have accreted at a relatively high rate in the early stages of their evolution, if black holes of $M_{\text{BH}} \gtrsim 10^9 M_{\odot}$ were already radiating at $z \approx 6.4$ [257, 266, 274]. From the low- z data, it is tempting to understand the Eddington ratio as the age of an AGN within its total lifetime (i.e., considering the totality of the time spent by a black hole as a “switched on” AGN): AGNs with steep X-ray spectra, strong FeII, and weak $[\text{OIII}]\lambda 5007$ are AGNs in an early phase of their evolution, which proceeds roughly from the lower left corner ($L_{\text{bol}}/L_{\text{Edd}} \rightarrow 1$) of the optical plane of E1 toward the upper right corner (low $L_{\text{bol}}/M_{\text{BH}}$, large M_{BH}). In this hypothetical scenario local NLSy1s are the “seedlings” of AGNs [229, 88]. Several results and correlations associated to the optical E1 can be explained by an evolutionary sequence. RL seem to be systematically more massive than RQ sources. They also radiate at lower $L_{\text{bol}}/L_{\text{Edd}}$. They show extended NLRs with large $W([\text{OIII}]\lambda\lambda 4959, 5007)$. At the other end we have “blue outliers” which are Pop. A sources with strong winds. Young AGNs still possess a compact NLR; they may have plenty of fuel and may show spectral evidence of circum-nuclear Starbursts. More massive, evolved systems may have less fuel and have had all the time to ionize interstellar clouds in the bulge of their host galaxies as well as to produce radio lobes exceeding the host galaxy size. Dying quasars have a limited gas supply surrounding their continuum-emitting regions, and may at best produce emission lines through the illumination of a last “strip” or ring of optically thick material as it may be the case of double-peakers. In this sense, the $L_{\text{bol}}/L_{\text{Edd}}$ sequence of E1 becomes literally an age sequence.

8.4 The Baldwin Effect

It is important to stress that the Baldwin effect is a very loose correlation between specific luminosity and $\text{CIV}\lambda 1549$ equivalent width. Claims and counter-claims of a Baldwin effect on the basis of small samples (few tens of objects) are unreliable [229]; the statistical weakness of the Baldwin correlation implies that the effect becomes appreciable only if a very large range in luminosity is considered, 4 – 6 decades. As pointed out by Sulentic et al. [229], results until mid-1999 have led to a standard scenario in which the Baldwin effect occurs in all measurable HILs except $\text{NV}\lambda 1240$, and the slope of the Baldwin relationship (i.e., $W(\text{CIV}\lambda 1549) \propto L_{\nu}^{-a}$, [5]) increases with ionization potential (e.g. [168]; see Ref. [96] for the implications of the apparent lack of any Baldwin effect for $\text{NV}\lambda 1240$). These

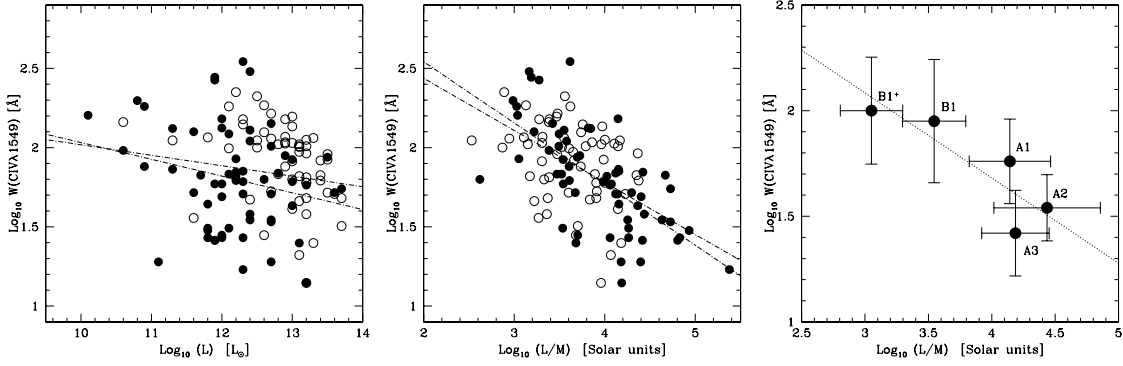


Figure 16: The Baldwin effects in the HST based sample of Bachev et al. [4]. Left panel: dependence of rest-frame $W(\text{CIV}\lambda 1549_{\text{BC}})$ on bolometric luminosity. Middle panel: dependence of $W(\text{civbc})$ on the L/M ratio (in solar units). Filled circles indicate RQ, open circles RL sources. Right Panel, same as middle panel but with median averages with the spectral types defined according to Ref. [230].

results have been basically confirmed by more recent studies based on large quasar samples [54, 59, 198], LBQS [87] and SDSS [285] included. A source of dispersion involves low-luminosity objects that have low $W(\text{CIV}\lambda 1549) \sim 10 \div 30 \text{\AA}$ since they tend to blur even more the Baldwin relationship. These sources are NLSy1s that preferentially occupy the lower left part of a $\log W$ vs. $\log L$ diagram.

Claims of a Baldwin effect on $\text{MgII}\lambda 2800$ should be taken somewhat with care [285], since the underlying FeII_{UV} emission can be very strong as well as variable from source to source depending on the BLR physical conditions, and the FeII_{UV} behavior has a function of luminosity and redshift is still poorly understood. Similar claims for $W(\text{H}\beta_{\text{BC}})$ have been rather erratic and unconvincing due to small sample sizes and large intrinsic scatter (Refs. [146, 229] found no trend; Ref. [162, 273] did).

The $[\text{OIII}]\lambda\lambda 4959, 5007$ lines seem to decrease in equivalent width with increasing luminosity [59, 162, 233, 285]. In the joint data of Refs. [233] and [140] there is definitely a significant correlation. Even if a luminosity correlation may not be always detectable (we stress again that the luminosity range must be very large) weak or no $[\text{OIII}]\lambda\lambda 4959, 5007$ seems to be a common property of many luminous AGNs [162, 287]. The reason why $[\text{OIII}]\lambda\lambda 4959, 5007$ seem to experience a Baldwin effect is presently not clear. It is possible that the $[\text{OIII}]\lambda\lambda 4959, 5007$ luminosity is limited by the physical size of the NLR [162], or that we are seeing an evolutionary effect at high- z , making high- z sources more similar to low- z Pop. A AGNs.

8.4.1 The Baldwin Effect as an Evolutionary Effect

A recent analysis of 80 PG quasars and one of ≈ 120 HST archive spectra indicates a strong correlation of $W(\text{CIV}\lambda 1549)$ with some of the emission parameters which define E1. Since

$L_{\text{bol}}/L_{\text{Edd}}$ drives the E1 correlations, $L_{\text{bol}}/L_{\text{Edd}}$ may be the primary physical parameter behind the Baldwin effect for C IV $\lambda 1549$ ([4, 11, 32]; Fig. 16). Also, high- z quasars show large C IV $\lambda 1549$ blueshifts like Pop. A sources at low- z [198, 233, 225]. Near-IR, low resolution spectra of eight of the most distant quasars (in the range $4.9 < z < 6.4$) show that half of these quasars are characterized by deep, broad and blueshifted absorption features typical of BAL quasars [135]. Similarities and close association between NLSy1, BAL QSOs, strong Fe II emission, and low W(C IV $\lambda 1549$) led to the suggestions that NLSy1s might be Seyfert galaxies in their early stage of evolution and as such may be low-redshift, low-luminosity analogues of high-redshift quasars [144, 229]. The C IV $\lambda 1549$ profiles show decreasing equivalent widths with increasing luminosity and the line profiles become similar to the “trapezoidal” shapes often observed in low- z NLSy1s [266]. However, a direct comparison of composite spectra of NLSy1 and $z \sim 4$ quasars through a PCA suggests that high- z quasi-stellar objects do not show a strong preference toward NLSy1 behavior [46]. Since this result is sample dependent and the mass-luminosity diagram of quasars can be similar up to $z \sim 2.5$ [48], it is still debatable whether evolution of $L_{\text{bol}}/L_{\text{Edd}}$ with z , selection effects or a combination of both may lead to the Baldwin effect [229]. After all, we are not observing other evolutionary effects even at $z \approx 6$. What seems unlikely is that the driving parameter of the Baldwin effect is M_{BH} [265]. Computing M_{BH} employing FWHM(C IV $\lambda 1549$) and assuming virial motions does not demonstrate that M_{BH} is driving the Baldwin effect because it is assumed to be $M_{\text{BH}} \propto L^{0.7}$, and this assumption leads, in part, to circular reasoning.

8.5 Quasars as Standard Candles

The Supernova Cosmology Project results supporting a cosmological constant $\Lambda \neq 0$ are still highly uncertain. The expected effect is just a few tens of magnitude at $z \approx 0.6$, and goes down to 0 at $z \approx 1.5$. A robust verification of a cosmological model with relative energy density $\Omega_{\text{M}} \approx 0.28$ and $\Omega_{\Lambda} \approx 0.72$ would require accurate measurements of standard candles in the range $0.6 \lesssim z \lesssim 3$, as it can be seen from the Hubble diagram with type Ia supernovae [200, 201].

It is clear from the previous discussion that, *at high z , we are observing quasars that can be very similar to the AGNs we are observing at low z , in terms of line width, Fe II prominence, HIL equivalent widths.* Trends with $L_{\text{bol}}/M_{\text{BH}}$ are much better defined than trends with luminosity. Luminosity effects remain weak and prone to sample bias (see, for example, Fig. 16, where the Baldwin effect is not significant while W(C IV $\lambda 1549$) shows a significant correlation with $L_{\text{bol}}/L_{\text{Edd}}$). Furthermore, $L_{\text{bol}}/L_{\text{Edd}}$ seems to affect many parameters related to physics and structure of the BLR, from LIL widths to HIL shifts and ionization degree. It makes therefore sense to use E1 correlations to estimate $L_{\text{bol}}/M_{\text{BH}}$. If M_{BH} is known with reasonable accuracy, it may become possible to retrieve z -independent information on L_{bol} . In principle, this can be achieved through two methods:

- a multivariate analysis which isolates the best linear combination of variables which are dependent only on $L_{\text{bol}}/M_{\text{BH}}$ and M_{BH} [279];

- an extension of the E1 diagram to high luminosity and high z [141].

Instruments like the infrared spectrometers mounted on 10-m sized telescopes make possible observations of intermediate redshift quasars ($1 \lesssim z \lesssim 2.2$) with S/N and resolution sufficient to apply the same data analysis procedure used for optical spectra of sources with $z \lesssim 1$. If these data are available, it is possible to measure the E1 parameters and to build an extension of “optical” E1 diagram. To fully exploit the E1 diagram, orientation needs to be estimated on an object-by-object basis. In the case of a radiation pressure driven wind, the CIV λ 1549 shift and profile shape should be sensitive to both $L_{\text{bol}}/M_{\text{BH}}$ and θ . Therefore, CIV λ 1549 measurements may provide an independent estimate of orientation, and hence a 3D observational parameter space to map into a 3D physical space ($\theta, L_{\text{bol}}/M_{\text{BH}}, M_{\text{BH}}$) which will ultimately yield a redshift-independent estimate of the luminosity (if an accurate low- z calibration can be defined). Merging results on M_{BH} and on L_{bol} from the previous analysis, it is reasonable to infer that, if θ is known within $\pm 5^\circ$, errors could be $\sim 60\%$ on M_{BH} , 80% on $L_{\text{bol}}/M_{\text{BH}}$. If errors are distributed randomly, an uncertainty as high as $\Delta m \approx 1$ could be farther reduced if samples of sources within a spectral type are averaged, yielding valuable data points for the Hubble diagram.

9 Conclusion

The main purpose of this paper was to point out how it is becoming possible to measure accretion parameters (especially M_{BH} and $L_{\text{bol}}/M_{\text{BH}}$) of AGNs. We highlighted major results and sources of uncertainty, as well as the connections between M_{BH} and $L_{\text{bol}}/L_{\text{Edd}}$, the structure of the broad line emitting region, and physical evolution. If we compare our present knowledge to the one of about 10 years ago, we can see an impressive progress. M_{BH} determinations through the virial assumption have become widely popular, and have been applied to quasars at all known z , up to 6.4, even if several sources of uncertainty limit strongly the accuracy by which M_{BH} is known for individual objects. It has been possible to show that many line properties and trends (including the Baldwin effect) correlate with $L_{\text{bol}}/L_{\text{Edd}}$, and the BLR structure is strongly affected by $L_{\text{bol}}/L_{\text{Edd}}$ through E1. There is no doubt that we have a much better framework with a strong observational support to understand the BLR structure, minority objects like “double-peakers” and BAL QSOs, and source evolution. Improvements on M_{BH} and $L_{\text{bol}}/M_{\text{BH}}$ estimates are possible through new multivariate analysis including orientation sensitive parameters, or through disk and wind BLR models accounting for the combined effects on line parameters of orientation and physics. We may be able to achieve a satisfactory vision of quasar structural evolution (not to mention boundaries on cosmography) well before the emitting regions may be resolved through space interferometry missions (e.g., Ref. [245]).

We thank Dr. Massimo Calvani for a careful reading of the manuscript.

References

- [1] Antonucci, R. 1993, *ARAAP*, **31**, 473
- [2] Aoki, K., Kawaguchi, T., & Ohta, K. 2004, ArXiv Astrophysics e-prints, astro-ph/0409546
- [3] Bachev, R. 1999, *AAP*, **348**, 71
- [4] Bachev, R., Marziani, P., Sulentic, J. W., Zamanov, R., Calvani, M., & Dultzin-Hacyan, D. 2004, *ApJ*, **617**, 171
- [5] Baldwin, J. A. 1977, *ApJ*, **214**, 679
- [6] Baldwin, J. A., Ferland, G. J., Korista, K. T., Hamann, F., & LaCluyzé, A. 2004, *ApJ*, **615**, 610
- [7] Baldwin, J., Ferland, G., Korista, K., & Verner, D. 1995, *ApJL*, **455**, L119
- [8] Bardeen, J.M., & Petterson, J.A., 1975, *ApJL*, **195**, 65
- [9] Barth, A. J., Martini, P., Nelson, C. H., & Ho, L. C. 2003, *ApJL*, **594**, L95
- [10] Barvainis, R., Lehar, J., Birkinshaw, M., Falke, H., & Blundell, K. M. 2004, ArXiv Astrophysics e-prints, astro-ph/0409554
- [11] Baskin, A. & Laor, A. 2004, *MNRAS*, **350**, L31
- [12] Baskin, A. & Laor, A. 2004, ArXiv Astrophysics e-prints, astro-ph/0409196
- [13] Becker, R. H., White, R. L., & Helfand, D. J. 1995, *ApJ*, **450**, 559
- [14] Bian, W., & Zhao, Y. 2002, *AAP*, **395**, 465
- [15] Bicknell, G. V. 2002, *New Astronomy Review*, **46**, 365
- [16] Blandford, R. D., Netzer, H., Woltjer, L., Courvoisier, T. J.-L., & Mayor, M. 1990, *Saas-Fee Advanced Course 20*. Lecture Notes 1990. Swiss Society for Astrophysics and Astronomy, XII, 280 pp. 97 figs.. Springer-Verlag Berlin Heidelberg New York,
- [17] Blandford, R. D., & Znajek, R. L. 1977, *MNRAS*, **179**, 433
- [18] Boller, Th., Brandt, W.N., Fink, H.H., 1996, *AAP*, **305**, 53 (BBF96)
- [19] Boller, Th., Brandt, W.N., Fabian, A.C. & Fink, H.H., 1997, *MNRAS*, **289**,393-405
- [20] Boller, T., Gallo, L. C., Lutz, D., & Sturm, E. 2002, *MNRAS*, **336**, 1143
- [21] Boroson, T. A. 2002, *ApJ*, **565**, 78

-
- [22] Boroson T.A., Green R.F., 1992, *ApJS* **80**, 190
- [23] Boroson, T. A. & Meyers, K. A. 1992, *ApJ*, **397**, 442
- [24] Boroson, T. A., & Oke, J. B. 1987, *PASP*, **99**, 809
- [25] Bottorff, M., Korista, K. T., Shlosman, I., & Blandford, R. D. 1997, *ApJ*, **479**, 200
- [26] Braitto, V., et al. 2004, *AAp*, **420**, 79
- [27] Breeveld, A. A., Puchnarewicz, E. M., & Otani, C. 2001, *MNRAS*, **325**, 772
- [28] Brinkmann, W., Papadakis, I. E., Ferrero, E., 2004, *AAp*, **414**, 107
- [29] Brotherton, M. S. 1996, *ApJS*, **102**, 1
- [30] Brotherton, M. S., Wills, B. J., Steidel, C. C., & Sargent, W. L. W. 1994, *ApJ*, **423**, 131
- [31] Brotherton, M. S., Wills, B. J., Francis, P. J., & Steidel, C. C. 1994, *ApJ*, **430**, 495
- [32] Calvani, M., Marziani, P., Bachev, R., Sulentic, J. W., Zamanov, R. K., & Dultzin-Hacyan, D. 2004, *Memorie della Societa Astronomica Italiana Supplement*, **5**, 223
- [33] Calvani, M., Marziani, P., & Sulentic, J. 1997, *Memorie della Societa Astronomica Italiana*, **68**, 93
- [34] Camenzind, M. 2004, ArXiv Astrophysics e-prints, astro-ph/0411573
- [35] Camenzind, M., & Krockenberger, M. A. 1992, *AAp*, **255**, 59
- [36] Capetti, A., Axon, D. J., Macchetto, F., Sparks, W. B., & Boksenberg, A. 1996, *ApJ*, **469**, 554
- [37] Caproni A., Abraham Z., 2004, *ApJ*, **602**, 625
- [38] Chen, K., & Halpern, J. P. 1989, *ApJ*, **344**, 115
- [39] Chiang, J., & Murray, N. 1996, *ApJ*, **466**, 704
- [40] Collier, S., et al. 2001, *ApJ*, **561**, 146
- [41] Collin, S., Boisson, C., Mouchet, M., Dumont, A.-M., Coupé, S., Porquet, D., & Rokaki, E. 2002, *AAp*, **388**, 771
- [42] Collin, S., & Hur, J.-M. 2001, *AAp*, **372**, 50
- [43] Collin, S., & Joly, M. 2000, *New Astronomy Review*, **44**, 531
- [44] Collin-Souffrin, S., Dyson, J. E., McDowell, J. C., & Perry, J. J. 1988, *MNRAS*, **232**, 539

- [45] Comastri, A., Setti, G., Zamorani, G., Elvis, M., Giommi, P., Wilkes, B.J., & McDowell, J.C. 1992, *ApJ*, **384**, 62
- [46] Constantin, A., & Shields, J. C. 2003, *PASP*, **115**, 592
- [47] Conway, J. E., & Wrobel, J. M. 1995, *ApJ*, **439**, 98
- [48] Corbett, E. A., et al. 2003, *MNRAS*, **343**, 705
- [49] Corbin, M. R. 1997, *ApJ*, **485**, 517
- [50] Corbin, M. R., & Boroson, T. A. 1996, *ApJS*, **107**, 69
- [51] Crenshaw, D.M., et al. 1996, *ApJ*, **470**, 322
- [52] Crenshaw, D. M., et al. 2002, *ApJ*, **566**, 187
- [53] Cresci, G., Maiolino, R., Marconi, A., Mannucci, F., & Granato, G. L. 2004, *AAp*, **423**, L13
- [54] Croom, S. M., et al. 2002, *MNRAS*, **337**, 275
- [55] Czerny, B., Niłołajuk, M., Piasecki, M., & Kuraszkiewicz, J. 2001, *MNRAS*, **325**, 865
- [56] Czerny, B., Rózańska, A., & Kuraszkiewicz, J. 2004, *AAp*, **428**, 39
- [57] Davies, R. I., Tacconi, L. J., & Genzel, R. 2004, *pJ*, **613**, 781
- [58] Dietrich, M., Hamann, F., Appenzeller, I., & Vestergaard, M. 2003, *ApJ*, **596**, 817
- [59] Dietrich, M., Hamann, F., Shields, J. C., Constantin, A., Vestergaard, M., Chaffee, F., Foltz, C. B., & Junkkarinen, V. T. 2002, *ApJ*, **581**, 912
- [60] Dietrich, M., & Hamann, F. 2004, *ApJ*, **611**, 761
- [61] Dong, X., Zhou, H., Wang, T., Wang, J., Li, C., & Zhou, Y. 2004, ArXiv Astrophysics e-prints, astro-ph/0411171
- [62] Dultzin-Hacyan, D., Marziani, P., & Sulentic, J. W. 2000, *Revista Mexicana de Astronomia y Astrofisica Conference Series*, **9**, 308
- [63] Dunlop, J. S., McLure, R. J., Kukula, M. J., Baum, S. A., O'Dea, C. P., & Hughes, D. H. 2003, *MNRAS*, **340**, 1095
- [64] Elvis, M. 2000, *ApJ*, **545**, 63
- [65] Elvis, M., et al. 1994, *ApJS*, **95**, 1
- [66] Eracleous, M., et al. 1997, *ApJ*, **490**, 216.

-
- [67] Eracleous, M., & Halpern, J. P. 2003, *ApJ*, **599**, 886
- [68] Eracleous, M., Halpern, J. P., Storchi-Bergmann, T., Filippenko, A. V., Wilson, A. S., & Livio, M. 2004, ArXiv Astrophysics e-prints, astro-ph/0404506
- [69] Fabian, A. C. 1979, *Royal Society of London Proceedings Series A*, **366**, 449
- [70] Falcke, H., Wilson, A. S., & Simpson, C. 1998, *ApJ*, **502**, 199
- [71] Ferland, G. J. 2000, *Revista Mexicana de Astronomia y Astrofisica Conference Series*, **9**, 153
- [72] Ferrarese, L., & Merritt, D. 2000, *ApJL*, **539**, L9
- [73] Floyd, D. J. E., Kukula, M. J., Dunlop, J. S., McLure, R. J., Miller, L., Percival, W. J., Baum, S. A., & O'Dea, C. P. 2004, *MNRAS*, **355**, 196
- [74] Forster, K., & Halpern, J. P. 1996, *ApJ*, **468**, 565
- [75] Freeman, P. E., Doe, S., Siemiginowska, A. 2001, SPIE Proceedings vol.4477, 76
- [76] Francis, P. J., Drake, C. L., Whiting, M. T., Drinkwater, M. J., & Webster, R. L. 2001, *Publications of the Astronomical Society of Australia*, **18**, 221
- [77] Francis, P. J., Hewett, P. C., Foltz, C. B., Chaffee, F. H., Weymann, R. J., & Morris, S. L. 1991, *ApJ*, **373**, 465
- [78] Freudling, W., Corbin, M. R., & Korista, K. T. 2003, *ApJL*, **587**, L67
- [79] Gallo, L.C., Boller, Th., Tanaka, Y., Fabian, A.C., Brandt, W.N., Welsh, W.F., Anabuki, N. & Haba, Y., 2004, *MNRAS*, **347**, 269-276
- [80] Gammie, C. F., Shapiro, S. L., & McKinney, J. C. 2004, *ApJ*, **602**, 312
- [81] Garcia-Barreto, J. A., Franco, J., Guichard, J., & Carrillo, R. 1995, *ApJ*, **451**, 156
- [82] Gaskell, C. M. 1996, *ApJ*, **464**, L107
- [83] Gaskell, C. M., Goosmann, R. W., Antonucci, R. R. J., & Whyson, D. H. 2004, *ApJ*, **616**, 147
- [84] Ghisellini, G., Padovani, P., Celotti, A., & Maraschi, L. 1993, *ApJ*, **407**, 65
- [85] Gierlinski & Done, C., 2004, *MNRAS*, **349**, L7
- [86] Giveon, U., Maoz, D., Kaspi, S., Netzer, H., & Smith, P. S. 1999, *MNRAS*, **306**, 637
- [87] Green, P. J., Forster, K., & Kuraszkiewicz, J. 2001, *ApJ*, **556**, 727
- [88] Grupe, D. 2004, *AJ*, **127**, 1799

- [89] Grupe, D., Beuermann, K., Mannheim, K., & Thomas, H.-C. 1999, *AAp*, **350**, 805
- [90] Grupe, D., Beuermann, K., Thomas, H.-C., Mannheim, K., & Fink, H. H. 1998, *AAp*, **330**, 25
- [91] Grupe, D., Thomas, H.-C., & Beuermann, K. 2001, *AAp*, **367**, 470
- [92] Gu, M., Cao, X., & Jiang, D. R. 2001, *MNRAS*, **327**, 1111
- [93] Gu, Q., Dultzin-Hacyan, D., & de Diego, J. A. 2001, *Revista Mexicana de Astronomia y Astrofisica*, **37**, 3
- [94] Haiman, Z., Quataert, E., & Bower, G. C. 2004, *ApJ*, **612**, 698
- [95] Halpern, J. P., Eracleous, M., Filippenko, A. V., & Chen, K. 1996, *ApJ*, **464**, 704
- [96] Hamann, F., & Ferland, G. 1999, *ARAAP*, **37**, 487
- [97] Hartig, G. F. & Baldwin, J. A. 1986, *ApJ*, **302**, 64
- [98] Hes, R., Barthel, P. D., & Fosbury, R. A. E. 1993, *Nature*, **362**, 326
- [99] Ho, L. C. 2002, *ApJ*, **564**, 120
- [100] Horne, K., Peterson, B. M., Collier, S. J., & Netzer, H. 2004, *PASP*, **116**, 465
- [101] Hughes, S. A. & Blandford, R. D. 2003, *ApJL*, **585**, L101
- [102] Imanishi, M., & Wada, K. 2004, *ApJ*, **617**, 214
- [103] Iwamuro, F., Kimura, M., Eto, S., Maihara, T., Motohara, K., Yoshii, Y., & Doi, M. 2004, *ApJ*, **614**, 69
- [104] Iwamuro, F., Motohara, K., Maihara, T., Kimura, M., Yoshii, Y., & Doi, M. 2002, *ApJ*, **565**, 63
- [105] Jarvis, M. J., & McLure, R. J. 2002, *MNRAS*, **336**, L38
- [106] Joly, M. 1991, *AAp*, **242**, 49
- [107] Joly, M. 1987, *AAp*, **184**, 33
- [108] Kaspi, S., Smith, P. S., Netzer, H., Maoz, D., Jannuzi, B. T., & Giveon, U. 2000, *ApJ*, **533**, 631
- [109] Kidger, M., Takalo, L., Sillanpää, A.: 1992, *AAp*, **264**, 32
- [110] Klimek, E.S., Gaskell, C.M. & Hedrick, C.H., 2004, *ApJ*, **609**, 69-79
- [111] Kollatschny, W. 2003, *AAp*, **412**, L61

-
- [112] Kollatschny, W. 2003, *AAp*, **407**, 461
- [113] Kollatschny, W., & Bischoff, K. 2002, *AAp*, **386**, L19
- [114] Kollatschny, W., Bischoff, K., Robinson, E.L., Welsh, W.F. & Hill, G.J., 2001, *AAp*, **379**, 125-135
- [115] Korista, K., Baldwin, J., Ferland, G., & Verner, D. 1997, *ApJS*, **108**, 401
- [116] Korista, K. T., & Goad, M. R. 2004, *ApJ*, **606**, 749
- [117] Korista, K. T., Voit, G. M., Morris, S. L., & Weymann, R. J. 1993, *ApJS*, **88**, 357
- [118] Krichbaum, T. P., et al. 2004, ArXiv Astrophysics e-prints, astro-ph/0411487
- [119] Krongold, Y., Dultzin-Hacyan, D., & Marziani, P. 2001, *AJ*, **121**, 702
- [120] Krongold, Y., Nicastro, F., Brickhouse, N. S., Elvis, M., Liedahl, D. A., & Mathur, S. 2003, *ApJ*, **597**, 832
- [121] Kuraszkievicz, J. K., Green, P. J., Crenshaw, D. M., Dunn, J., Forster, K., Vestergaard, M., & Aldcroft, T. L. 2004, *ApJS*, **150**, 165
- [122] Kuraszkievicz, J. K., Green, P. J., Forster, K., Aldcroft, T. L., Evans, I. N., & Koratkar, A. 2002, *ApJS*, **143**, 257
- [123] Krolik, J. H. 2001, *ApJ*, **551**, 72
- [124] Lacy, M., Laurent-Muehleisen, S. A., Ridgway, S. E., Becker, R. H., & White, R. L. 2001, *ApJL*, **551**, L17
- [125] Laor, A. 2000, *ApJL*, **543**, L111
- [126] Laor, A. 2001, *ApJ*, **553**, 677
- [127] Laor, A. 2003, *ApJ*, **590**, 86
- [128] Lehto, H. J., Valtonen, M. J., 1996, *ApJ* **460**, 207
- [129] Leighly, K. M. 1999, *ApJS*, **125**, 317
- [130] Leighly, K. M. 2004, *ApJ*, **611**, 125
- [131] Leighly, K. M., & Moore, J. R. 2004, *ApJ*, **611**, 107
- [132] Lewis, K. T., Eracleous, M., Halpern, J. P., & Storchi-Bergmann, T. 2004, ArXiv Astrophysics e-prints, astro-ph/0404342
- [133] Lipari, S., Terlevich, R., & Macchetto, F. 1993, *ApJ*, **406**, 451

- [134] Lobanov, A. P., & Roland, J. 2004, ArXiv Astrophysics e-prints, astro-ph/0411417
- [135] Maiolino, R., Oliva, E., Ghinassi, F., Pedani, M., Mannucci, F., Mujica, R., & Juarez, Y. 2004, *AAp*, **420**, 889
- [136] Marziani, P., & Sulentic, J. W. 1993, *ApJ*, **409**, 612
- [137] Marziani, P., Sulentic, J. W., Calvani, M., Perez, E., Moles, M., & Penston, M. V. 1993, *ApJ*, **410**, 56
- [138] Marziani P., Sulentic J.W., Dultzin-Hacyan D., Calvani M., Moles M., 1996, *ApJS* **104**, 37
- [139] Marziani P., Sulentic J.W., Zwitter T., Dultzin-Hacyan D., Calvani M., 2001, *ApJ*, **558**, 553 (M01)
- [140] Marziani P., Sulentic J. W., Zamanov R., Calvani M., Dultzin-Hacyan D., Bachev R., Zwitter T., 2003a, *ApJS*, **145**, 199 (M03)
- [141] Marziani, P., Sulentic, J. W., Zamanov, R., Calvani, M., Della Valle, M., Stirpe, G., & Dultzin-Hacyan, D. 2003, *Memorie della Societa Astronomica Italiana Supplement*, **3**, 218
- [142] Marziani, P., Zamanov, R., Sulentic, J. W., Dultzin-Hacyan, D., Bongardo, C., & Calvani, M. 2003b, *ASP Conf. Ser. 290: Active Galactic Nuclei: From Central Engine to Host Galaxy*, **229**
- [143] Marziani P., Zamanov R., Sulentic J. W., Calvani M., 2003c, *MNRAS*, **345**, 1133 S. 2000, *MNRAS*, **314**, L17
- [144] Mathur, S. 2000, *MNRAS*, **314**, L17
- [145] Mathur, S., Kuraszkievicz, J., & Czerny, B. 2001, *New Astronomy*, **6**, 321
- [146] McIntosh, D. H., Rieke, M. J., Rix, H.-W., Foltz, C. B., & Weymann, R. J. 1999, *ApJ*, **514**, 40
- [147] McLure, R. J., & Dunlop, J. S. 2001, *MNRAS*, **327**, 199
- [148] McLure, R. J., & Dunlop, J. S. 2002, *MNRAS*, **331**, 795
- [149] McLure, R. J., & Dunlop, J. S. 2004, *MNRAS*, **352**, 1390
- [150] McLure, R. J., & Jarvis, M. J. 2002, *MNRAS*, **337**, 109
- [151] McLure, R. J., & Jarvis, M. J. 2004, *MNRAS*, **353**, L45
- [152] Merloni, A., Heinz, S., & di Matteo, T. 2003, *MNRAS*, **345**, 1057

-
- [153] Miller, H.R. Ferrara, E.C., McFarland, J.P., Wilson, J.W., Daya, A.B., Fried, R.E., 2000, *New Astron. Rev.*, **44**, 539
- [154] Moran, E. C., Halpern, J. P., & Helfand, D. J. 1996, *ApJS*, **106**, 341
- [155] Murray, N., & Chiang, J. 1997, *ApJ*, **474**, 91
- [156] Murtagh, F. & Heck, A. 1987, *Astrophysics and Space Science Library, Dordrecht: Reidel*, 1987
- [157] Mushotzki, R.F., Done, C., Pounds, K.A., 1993, *ARAAP*, **31**, 717
- [158] Nagao, T., Murayama, T. & Taniguchi, Y., 2001, *ApJ*, **546**, 744-758
- [159] Narayan, R. 2004, ArXiv Astrophysics e-prints, astro-ph/0411385
- [160] Nelson, C. H., Green, R. F., Bower, G., Gebhardt, K., & Weistrop, D. 2004, *ApJ*, **615**, 652
- [161] Nelson, C. H. 2000, *ApJL*, **544**, L91
- [162] Netzer, H., Shemmer, O., Maiolino, R., Oliva, E., Croom, S., Corbett, E., & di Fabrizio, L. 2004, *ApJ*, **614**, 558
- [163] Newman, J. A., Eracleous, M., Filippenko, A. V., & Halpern, J. P. 1997, *ApJ*, **485**, 570
- [164] Nicastro, F. 2000, *ApJL*, **530**, L65
- [165] Nicastro, F., Martocchia, A., & Matt, G. 2003, *ApJL*, **589**, L13
- [166] Onken, C. A., Ferrarese, L., Merritt, D., Peterson, B. M., Pogge, R. W., Vestergaard, M., & Wandel, A. 2004, *ApJ*, **615**, 645
- [167] Oshlack, A. Y. K. N., Webster, R. L., & Whiting, M. T. 2002, *ApJ*, **576**, 81
- [168] Osmer, P. S., & Shields, J. C. 1999, *Astronomical Society of the Pacific Conference Series*, **162**, 235
- [169] Netzer, H. 2003, *ApJL*, **583**, L5
- [170] Netzer, H. 1990, in Blandford, R. D., Netzer, H., Woltjer, L., Courvoisier, T. J.-L., & Mayor, M. 1990, *Saas-Fee Advanced Course 20*. Lecture Notes 1990. *Swiss Society for Astrophysics and Astronomy, XII*, **280** pp. 97 Springer-Verlag Berlin Heidelberg New York,
- [171] Ostorero, L.; Villata, M.; Raiteri, C. M. 2004, *AAP*, **419**, 913.
- [172] Osterbrock, D.E., Pogge, R.W., 1985, *ApJ*, **297**, 166

- [173] Padovani, P., Allen, M. G., Rosati, P., & Walton, N. A. 2004, *AAp*, **424**, 545
- [174] Page, K. L., Reeves, J. N., O'Brien, P. T., Turner, M. J. L., & Worrall, D. M. 2004, *MNRAS*, **353**, 133
- [175] Paul C., Brotherton M.S., Diamond-Stanic A.), Vanden Berk D., Canalizo G. 2005, BAAS, in press
- [176] Peterson, B. M. 1993, *PASP*, **105**, 247
- [177] Peterson, B. M. 1997, *An introduction to active galactic nuclei*, Cambridge, New York Cambridge University Press, 1997
- [178] Peterson, B. M. 2004, ArXiv Astrophysics e-prints, astro-ph/0404539
- [179] Peterson, B. M., et al. 2004, *ApJ*, **613**, 682
- [180] Peterson, B.M., et al. 2000, *ApJ*, **542**, 161
- [181] Peterson, B. M., et al. 2002, *ApJ*, **581**, 197
- [182] Peterson, B. M. & Horne, K. 2004, ArXiv Astrophysics e-prints, astro-ph/0407538
- [183] Peterson, B.M., Korista, K.T., & Wagner, R.M., 1989, *AJ*, **98**, 100
- [184] Peterson, B. M., Wanders, I., Horne, K., Collier, S., Alexander, T., Kaspi, S., & Maoz, D. 1998, *PASP*, **110**, 660
- [185] Pica, A.J., Smith, A.G., Webb, J.R., Leacock, R.J., Clements, S., & Gombola, P.P. 1988, *AJ*, **96**, 1215
- [186] Piconcelli, E., Jimnez-Bailon, E., Guainazzi, M., et al., 2004, *MNRAS*, **351**, 161
- [187] Popović, L. Č., Mediavilla, E., Bon, E., & Ilić, D. 2004, *AAp*, **423**, 909
- [188] Popović, L. Č. 2003, *ApJ*, **599**, 140
- [189] Porquet, D., Reeves, J. N., O'Brien, P., & Brinkmann, W. 2004, *AAp*, **422**, 85
- [190] Proga, D., Stone, J. M., & Kallman, T. R. 2000, *ApJ*, **543**, 686
- [191] Pounds, K. A., King, A. R., Page, K. L., & O'Brien, P. T. 2003, *MNRAS*, **346**, 1025
- [192] Pounds, K. A., Reeves, J. N., King, A. R., Page, K. L., O'Brien, P. T., & Turner, M. J. L. 2003, *MNRAS*, **345**, 705
- [193] Pounds, K. A., Reeves, J. N., Page, K. L., Edelson, R., Matt, G., & Perola, G. C. 2003, *MNRAS*, **341**, 953

-
- [194] Pursimo, T., Takalo, L.O., Sillanpää, A., Kidger, M., Lethto, H.J., Heidt, J., Charles, P.A., Aller, H., Aller, M., Beckmann, V., and 61 coauthors, 2000, *AApS*, **146**, 141.
- [195] Reeves, J. N., & Turner, M. J. L., 2000, *MNRAS*, **316**, 234
- [196] Reichard, T. A., et al. 2003, *AJ*, **125**, 1711
- [197] Reichard, T. A., et al. 2003, *AJ*, **126**, 2594
- [198] Richards, G. T., Vanden Berk, D. E., Reichard, T. A., Hall, P. B., Schneider, D. P., SubbaRao, M., Thakar, A. R., & York, D. G. 2002, *AJ*, **124**, 1
- [199] Richards, G. T., et al. 2003, *AJ*, **126**, 1131
- [200] Riess, A. G. et al. 2001, *ApJ*, **560**, 49
- [201] Riess, A. G., et al. 2004, *ApJ*, **607**, 665
- [202] Rodríguez-Ardila, A., & Viegas, S. M. 2003, *MNRAS*, **340**, L33
- [203] Rodríguez-Pascual, P.M., Mas-Hesse, J.M., Santos-Lleo, M., 1997, *AAp*, **327**, 72
- [204] Rokaki, E., Lawrence, A., Economou, F., & Mastichiadis, A. 2003, *MNRAS*, **340**, 1298
- [205] Romano, P., Turner, T. J., Mathur, S., & George, I. M. 2002, *ApJ*, **564**, 162
- [206] Ross, R. R., & Fabian, A. C. 1993, *MNRAS*, **261**, 74
- [207] Saslaw, W. C., Waltonen, M. J., & Aarseth, S. J. 1974, *ApJ*, **190**, 253
- [208] Schneider, D. P., et al. 2002, *AJ*, **123**, 567
- [209] Scott, J. E., Kriss, G. A., Brotherton, M., Green, R. F., Hutchings, J., Shull, J. M., & Zheng, W. 2004, *ApJ*, **615**, 135
- [210] <http://www.sdss.org>
- [211] Shakura, N. I., & Sunyaev, R. A. 1973, *AAp*, **24**, 337
- [212] Shang, Z., et al. 2004, ArXiv Astrophysics e-prints, astro-ph/0409697
- [213] Shang, Z., Wills, B. J., Robinson, E. L., Wills, D., Laor, A., Xie, B., & Yuan, J. 2003, *ApJ*, **586**, 52
- [214] Shields, J. C., Ferland, G. J., & Peterson, B. M. 1995, *ApJ*, **441**, 507
- [215] Stepanian, J. A., et al. 2003, *ApJ*, **588**, 746
- [216] Strateva, I. V., et al. 2003, *AJ*, **126**, 1720

- [217] Shapovalova, A.I., Burenkov, A.N., Carrasco, L., Chavushyan, V.H., Doroshenko, V.T., Dumont, A.M., Lyuty, V.M., Valds, J.R., Vlasuyk, V.V., Bochkarev, N.G., 2001, *AAp*, **376**, 775.
- [218] Shapovalova, A. I., et al. 2004, *AAp*, **422**, 925
- [219] Shields, G. A. 1996, *ApJL*, **461**, L9
- [220] Shields, G. A., Gebhardt, K., Salviander, S., Wills, B. J., Xie, B., Brotherton, M. S., Yuan, J., & Dietrich, M. 2003, *ApJ*, **583**, 124
- [221] Sigut, T. A. A., Pradhan, A. K., & Nahar, S. N. 2004, *ApJ*, **611**, 81
- [222] Sillanpää, A., et al. 1996, *A & A*, in press
- [223] Sillanpää, A., Haarala S., Valtonen M. J., Sundelius B., Byrd G. G., 1988, *ApJ*, **325**, 628.
- [224] Storchi-Bergmann, T., et al. 2003, *ApJ*, **598**, 956
- [225] Sulentic, J. W., Dultzin-Hacyan, D., Marziani, P., C. Bongardo, V. Braitto, M. Calvani, Zamanov, R., 2005, *RevMexAAp*, submitted
- [226] Sulentic, J. W. & Marziani, P. 1999, *ApJL*, **518**, L9
- [227] Sulentic, J. W., Marziani, P., & Calvani, M. 1998, *ApJL*, **497**, L65
- [228] Sulentic, J. W., Marziani, P., Zwitter, T., & Calvani, M. 1995, *ApJL*, **438**, L1
- [229] Sulentic, J. W., Marziani, P., & Dultzin-Hacyan, D. 2000a, *ARA&A*, **38**, 521
- [230] Sulentic, J. W., Marziani, P., Zamanov, R., Bachev, R., Calvani, M., & Dultzin-Hacyan, D. 2002, *ApJ*, **566**, L71
- [231] Sulentic, J. W., Marziani, P., Zwitter, T., Dultzin-Hacyan, D., & Calvani, M. 2000b, *ApJ*, **545**, L15
- [232] Sulentic, J. W., Marziani, P., Zwitter, T., Dultzin-Hacyan, D., & Calvani, M. 2000, *ApJL*, **545**, L15
- [233] Sulentic, J. W., Stirpe, G. M., Marziani, P., Zamanov, R., Calvani, M., & Braitto, V. 2004, *ArXiv Astrophysics e-prints*, astro-ph/0405279
- [234] Sulentic J. W., Zamfir S., Marziani P., Bachev R., Calvani M., Dultzin-Hacyan D., 2003, *ApJ*, **597**, L17
- [235] Sulentic, J. W., Zheng, W., Calvani, M., & Marziani, P. 1990, *ApJL*, **355**, L15
- [236] Tersranta, H., Valtaoja, E.: 1995, *Private Communication*

-
- [237] Thompson K. L., Hill G. J., Elston R. 1999, *ApJ*, **515**, 487
- [238] Thorne, K. S. 1974, *ApJ*, **191**, 507
- [239] Tolea, A., Krolik, J. H., & Tsvetanov, Z. 2002, *ApJL*, **578**, L31
- [240] Tran, H. D. 2001, *ApJL*, **554**, L19
- [241] Turner, T.J., George, I.M., Nandra, K., & Turcan, D., 1999, *ApJ*, **524**, 667
- [242] Turnshek, D. A. 1984, *ApJ*, **280**, 51
- [243] Turnshek, D. A., Monier, E. M., Sirola, C. J., & Espey, B. R. 1997, *ApJ*, **476**, 40
- [244] Ulrich, M.-H., Maraschi, L., & Urry, C.M., 1997, *ARAAP*, **35**, 445
- [245] Unwin, S. C., Wehrle, A. E., Jones, D. L., Meier, D. L., & Piner, B. G. 2002, *Publications of the Astronomical Society of Australia*, **19**, 5
- [246] Valtonen, M. J.; Lehto, H. J.; Pietil, H., 1999, *AAp*, **342**, 29.
- [247] Vanden Berk, D. E., et al. 2001, *AJ*, **122**, 549
- [248] Vaughan, S., Reeves, J., Warwick, R., & Edelson, R. 1999, *MNRAS*, **309**, 113
- [249] Verner, E., Bruhweiler, F., Verner, D., Johansson, S., & Gull, T. 2003, *ApJL*, **592**, L59
- [250] Verner, E., Bruhweiler, F., Verner, D., Johansson, S., Kallman, T., & Gull, T. 2004, *ApJ*, **611**, 780
- [251] Verner, E. M., & Peterson, B. A. 2004, *ApJL*, **608**, L85
- [252] Verner, E. M., Verner, D. A., Korista, K. T., Ferguson, J. W., Hamann, F., & Ferland, G. J. 1999, *ApJS*, **120**, 101
- [253] Véron-Cetty, M.-P. & Véron, P. 2003, *AAp*, **412**, 399
- [254] Véron-Cetty, M.-P., Véron, P., & Gonçalves, A. C. 2001, *AAp*, **372**, 730
- [255] Véron-Cetty, M.-P., Joly, M., & Véron, P. 2004, *AAp* **417**, 515
- [256] Vestergaard, M. 2002, *ApJ*, **571**, 733
- [257] Vestergaard, M. 2004, *ApJ*, **601**, 676
- [258] Vestergaard, M., & Wilkes, B. J. 2001, *ApJS*, **134**, 1
- [259] Vicente, L, et al., 1995, in *Extragalactic Radio Sources*, IAU symposium 175, Bologna.

- [260] Villata, M., & Raiteri, C. M. 1999, *AAp*, **347**, 30
- [261] Wampler, E. J. 1986, *AAp*, **161**, 223
- [262] Wandel, A., Peterson, B. M., & Malkan, M. A. 1999, *ApJ*, **526**, 579
- [263] Wang, T., Brinkmann, W., Bergeron, J., 1996, *AAp*, **309**, 81
- [264] Wang, T., & Zhang, X. 2003, *MNRAS*, **340**, 793
- [265] Warner, C., Hamann, F., & Dietrich, M. 2003, *ApJ*, **596**, 72
- [266] Warner, C., Hamann, F., & Dietrich, M. 2004, *ApJ*, **608**, 136
- [267] Webb, J.R., Smith, A.G., Leacock, R.J., Fitzgibbons, G.L., Gombola, P.P., & Shepherd, D.W. 1988, *AJ*, **95**, 374
- [268] Webb, W. & Malkan, M., 2000, *ApJ*, **540**, 652-677
- [269] Weymann R.J., Morris S.L., Foltz C.B., Hewett P.C., 1991, *ApJ* **373**, 23
- [270] Wang, T., & Zhang, X. 2003, *MNRAS*, **340**, 793
- [271] Whittle, M. 1992, *ApJS*, **79**, 49
- [272] Wilkes, B. J., & Elvis, M. 1987, *ApJ*, **323**, 243
- [273] Wilkes, B. J., Kuraszkiwicz, J., Green, P. J., Mathur, S., & McDowell, J. C. 1999, *ApJ*, **513**, 76
- [274] Willott, C. J., McLure, R. J., & Jarvis, M. J. 2003, *ApJL*, **587**, L15
- [275] Wills, B. J., & Browne, I. W. A. 1986, *ApJ*, **302**, 56
- [276] Wills, B. J., Netzer, H., & Wills, D. 1985, *ApJ*, **288**, 94
- [277] Wills, B. J., Brotherton, M. S., Fang, D., Steidel, C. C., & Sargent, W. L. W. 1993, *ApJ*, **415**, 563
- [278] Wills, B. J., Brandt, W. N., & Laor, A. 1999, *ApJL*, **520**, L91
- [279] Wills, B. J., & Shang, Z. 2004, *Advances in Space Research*, **34**, 2584
- [280] Wilson, A. S., & Colbert, E. J. M. 1995, *ApJ*, **438**, 62
- [281] Woo, J., & Urry, C. M. 2002, *ApJ*, **579**, 530
- [282] Woo, J., & Urry, C. M. 2002, *ApJ*, **581**, L5
- [283] Wu, X., & Liu, F. K. 2004, *ApJ*, **614**, 91

-
- [284] Wu, X.-B., Wang, R., Kong, M. Z., Liu, F. K., & Han, J. L. 2004, *AAp*, **424**, 793
- [285] Yip, C. W., et al. 2004, *AJ*, **128**, 2603
- [286] Young, A.J., Crawford, C.S., Fabian, A.C., Brandt, W.N., O'Brien, P.T., 1999, *MNRAS*, **304**, 4
- [287] Yuan, M. J. & Wills, B. J. 2003, *ApJL*, **593**, L11
- [288] Zamanov, R., Marziani, P., Sulentic, J. W., Calvani, M., Dultzin-Hacyan, D., & Bachev, R. 2002, *ApJL*, **576**, L9
- [289] Zamanov, R. & Marziani, P. 2002, *ApJL*, **571**, L77
- [290] Zheng, W., Kriss, G. A., Telfer, R. C., Grimes, J. P., & Davidsen, A. F. 1997, *ApJ*, **475**, 469
- [291] Zhou, H., Wang, T., Dong, X., Zhou, Y., & Li, C. 2003, *ApJ*, **584**, 147
- [292] Zhou, H., Wang, T., Dong, X., Li, C., & Zhang, X. 2004, ArXiv Astrophysics e-prints, astro-ph/0411252